

A Model of Supernovae Feedback in Galaxy Formation

G. Efstathiou

Institute of Astronomy, Madingley Road, Cambridge, CB3 0HA.

27 October 2018

ABSTRACT

A model of supernovae feedback during disc galaxy formation is developed. The model incorporates infall of cooling gas from a halo and outflow of hot gas from a multiphase interstellar medium (ISM). The star formation rate is determined by balancing the energy dissipated in collisions between cold gas clouds with that supplied by supernovae in a disc marginally unstable to axisymmetric instabilities. Hot gas is created by thermal evaporation of cold gas clouds in supernovae remnants, and criteria are derived to estimate the characteristic temperature and density of the hot component and hence the net mass outflow rate. A number of refinements of the model are investigated, including a simple model of a galactic fountain, the response of the cold component to the pressure of the hot gas, pressure induced star formation and chemical evolution. The main conclusion of this paper is that low rates of star formation can expel a large fraction of the gas from a dwarf galaxy. For example, a galaxy with circular speed $\sim 50 \text{ km s}^{-1}$ can expel $\sim 60\text{--}80\%$ of its gas over a time-scale of ~ 1 Gyr, with a star formation rate that never exceeds $\sim 0.1 M_{\odot}/\text{year}$. Effective feedback can therefore take place in a quiescent mode and does not require strong bursts of star formation. Even a large galaxy, such as the Milky Way, might have lost as much as 20% of its mass in a supernovae driven wind. The models developed here suggest that dwarf galaxies at high redshifts will have low average star formation rates and may contain extended gaseous discs of largely unprocessed gas. Such extended gaseous discs might explain the numbers, metallicities and metallicity dispersions of damped Lyman alpha systems.

1 INTRODUCTION

Since the pioneering paper of White and Rees (1978), it has been clear that some type of feedback mechanism is required to explain the shape of the galaxy luminosity function in hierarchical clustering theories. The reason for this is easy to understand; if the power spectrum of mass fluctuations is approximated as a power law $P(k) \propto k^n$, the Press-Schechter (1974) theory for the distribution of virialized haloes predicts a power law dependence at low masses

$$\frac{dN(m)}{dm} \propto m^{-(9-n)/6}. \quad (1)$$

For any reasonable value of the index n ($n \approx -2$ on the scales relevant to galaxy formation in cold dark matter (CDM) models), equation (1) predicts a much steeper mass spectrum than the observed faint end slope of the galaxy luminosity function, $dN(L)/dL \propto L^{\alpha}$, with $\alpha \approx -1$ (Efstathiou, Ellis and Peterson 1988, Loveday *et al.* 1992, Zucca *et al.* 1997). Furthermore, the cooling times of collisionally ionised gas clouds forming at high redshift are short compared to the Hubble time (Rees and Ostriker 1977, White and Rees 1978). Thus, in the absence of feedback, one would expect that a large fraction of the baryons would have collapsed at high redshift into low mass dark matter haloes, in contradiction with observations.

In reality, there are a number of complex physical mechanisms that can influence galaxy formation and these need to be understood if we are to construct a realistic model of galaxy formation. In the ‘standard’ cold dark matter model (*i.e.* nearly scale invariant adiabatic perturbations), the first generation of collapsed objects will form in haloes with low virial temperatures ($T \lesssim 10^4 \text{ K}$, characteristic circular speeds $v_c \lesssim 20 \text{ km s}^{-1}$). Molecular hydrogen is the dominant coolant at such low temperatures and so an analysis of the formation of the first stellar objects requires an understanding of the molecular hydrogen abundance and how this is influenced by the ambient ultraviolet radiation field (Haiman, Rees and Loeb 1997, Haiman, Abel and Rees 1999). As the background UV flux rises, the temperature of the intergalactic medium will rise to $\sim 10^4 \text{ K}$ (*e.g.* Gnedin and Ostriker 1997) and the UV background will reduce the effectiveness of cooling in low density highly ionized gas (Efstathiou 1992). A UV background can therefore suppress the collapse of gas in regions of low overdensity. It is this low density photoionized gas that we believe accounts for the Ly α absorption lines (Cen *et al.* 1994, Hernquist *et al.* 1996, Theuns *et al.* 1998, Bryan *et al.* 1999). Photoionization can also suppress the collapse of gas in haloes with circular speeds of up to $v_c \sim 20\text{--}30 \text{ km s}^{-1}$. However, numerical simulations have shown that a UV background cannot prevent the collapse of

arXiv:astro-ph/0002245v1 11 Feb 2000

gas in haloes with higher circular speeds, though it can reduce significantly the efficiency with which low density gas is accreted onto massive galaxies (Quinn, Katz and Efstathiou 1996, Navarro and Steinmetz 1997).

To explain the galaxy luminosity function, feedback is required in galaxies with circular speeds $v_c \gtrsim 50 \text{ km s}^{-1}$ with characteristic virial temperatures of $\gtrsim 10^5 \text{ K}$. Energy injection from supernovae is probably the most plausible feedback mechanism for systems with such high virial temperatures. Winds from quasars might also disrupt galaxy formation (Silk and Rees 1998) or, more plausibly, limit the growth of the central black hole (Fabian 1999). Here we will be concerned exclusively with supernova driven feedback and will not consider feedback from an active nucleus. Simple parametric models of supernovae feedback were developed by White and Rees (1978) and White and Frenk (1991) and form a key ingredient of semi-analytic models of galaxy formation (*e.g.* Kauffmann, White and Guiderdoni 1993, Lacey *et al.* 1993, Cole *et al.* 1994, Baugh *et al.* 1996, 1998, Somerville and Primack 1999). In this paper, we develop a more detailed model of the feedback process itself. Previous papers on supernovae feedback include those of Larson (1974), Dekel and Silk (1986) and Babul and Rees (1992). These authors compute the energy injected by supernovae into a uniform interstellar medium (ISM) and apply a simple binding energy criterion to assess whether the ISM will be driven out of the galaxy. The feedback process in these models is explosive, operating on the characteristic timescale of $\sim 10^6 - 10^7$ yrs for supernova remnants to overlap. This is much shorter than the typical infall timescale of hot gas in the halo, begging the question of how a reservoir of cold gas accumulated in the first place. The present paper differs in that we model the ISM as a two-phase medium consisting of cold clouds and a hot pressure confining medium, *i.e.* as a simplified version of the three-phase model of the ISM developed by McKee and Ostriker (1977, hereafter MO77). The cold component contains most of the gaseous mass of the disc and is converted into a hot phase by thermal evaporation in expanding supernovae remnants. In this type of model, the cold phase can be lost gradually in a galactic wind as it is slowly converted into a hot phase.

The main result of this paper is that low rates of star formation can expel a large fraction of the baryonic mass in dwarf galaxies over a relatively long timescale of ~ 1 Gyr. We therefore propose that effective feedback can operate in an steady, unspectacular mode; strong bursts of star formation and superwind-like phenomena (*e.g.* Heckman, Armus and Miley 1990) are not required, although galaxies may experience additional feedback of this sort. In fact, hydrodynamic simulations suggest that nuclear starbursts are ineffective in removing the ISM from galaxies with gas masses $\gtrsim 10^6 M_\odot$ (Mac Low and Ferrara 1999, Strickland and Stevens 1999) because hot gas generated in the nuclear regions is expelled in a bipolar outflow without coupling to the cool gas in the rest of the disc. This result provides additional motivation for investigating a “quiescent” mode of feedback. Silk (1997) describes a model which is similar, in some respects, to the model described here. However, the model described here is more detailed and allows a crude investigation of the radial properties of a disc galaxy during formation.

The layout of this paper is as follows. A simple model of star formation regulated by disc instabilities is described in Section 2. This is applied to ‘closed box’ (*i.e.* no infall or outflow of gas) models of disc galaxies neglecting feedback. Section 3 describes a model of the interaction of expanding supernovae shells in a two-phase ISM. This section is based on the model of MO77, but instead of focussing on equilibrium solutions that might apply to our own Galaxy, we compute the net rate of conversion of cold gas to hot gas incorporating the model for self-regulating star formation. This yields the temperature and density of the hot phase as a function of time and radius within the disc. Section 4 revisits the model of Section 2, but includes simultaneous infall and outflow of gas. This model is extended in Section 5 to include a galactic fountain, the pressure response of the cold ISM to the hot phase, and a model of chemical evolution. Section 6 describes some results from this model and discusses the effects of varying some of the input parameters. In addition, the efficiency of feedback is computed as a function of the circular speed of the surrounding dark matter halo. Our conclusions are summarized in Section 7. Although we focus on disc galaxies in this paper, a similar formalism could be applied to the formation of bulges if the assumption that gas conserves its angular momentum during collapse is relaxed.

2 STAR FORMATION REGULATED BY DISC INSTABILITIES

2.1 Rotation curve for the Disc and Halo

The dark halo is assumed to be described by the Navarro, Frenk and White (1996, hereafter NFW) profile

$$\rho_H(r) = \frac{\delta_c \rho_c}{(cx)(1+cx)^2}, \quad x \equiv r/r_v, \quad (2)$$

where ρ_c is the critical density, r_v is the virial radius at which the halo has a mean overdensity of 200 with respect to the background and c is a concentration parameter (approximately 10 for CDM models). The circular speed corresponding to this profile is

$$v_H^2(r) = v_v^2 \frac{1}{x} \frac{[\ln(1+cx) - cx/(1+cx)]}{[\ln(1+c) - c/(1+c)]}, \quad v_v^2 \equiv \frac{GM_v}{r_v}, \quad (3)$$

where M_v is the mass of the halo within the virial radius.

We assume that the disc surface mass density distribution is described by an exponential,

$$\mu_D(r) = \mu_0 \exp(-r/r_D), \quad M_D \equiv 2\pi\mu_0 r_D^2, \quad (4)$$

where M_D is the total disc mass. The rotation curve of a cold exponential disc is given by (Freeman 1970)

$$v_D^2(r) = 2v_c^2 y^2 [I_0(y)K_0(y) - I_1(y)K_1(y)], \quad (5)$$

$$y \equiv \frac{1}{2} \frac{r}{r_D}, \quad v_c^2 = \frac{GM_D}{r_D}.$$

To relate the disc scale length, r_D , to the virial radius of the halo r_v , we assume that the angular momentum of the disc material acquired by tidal torques is approximately conserved during the collapse of the disc (see Fall and Efstathiou 1980). This fixes the collapse factor

$$f_{coll} = \frac{r_v}{r_D} \quad (6)$$

in terms of the dimensionless spin parameter $\lambda_H \equiv J|E|^{1/2}G^{-1}M^{-5/2}$ of the halo component. The spin parameter is found to have a median value of ≈ 0.05 from N-body simulations (Barnes and Efstathiou 1987), and for the models described here, this value is reproduced for collapse factors of around 50. A more detailed calculation of the collapse factor of the disc is given in Section 4.

2.2 Vertical scale height of the disc

The velocity dispersion of the cold gas clouds in the vertical direction is assumed to be constant and equal to σ_g^2 . The equations of stellar hydrodynamics then give the following solution

$$\rho(z) = \frac{\mu_g}{2H_g} \operatorname{sech}^2\left(\frac{z}{H_g}\right), \quad (7)$$

where μ_g is the surface mass density of the gas and the scale height is given by

$$H_g = \frac{\sigma_g^2}{\pi G \mu_g}. \quad (8)$$

Equation (8) must be modified to take into account the stellar disc. We do this approximately by assuming ‘disc pressure equilibrium’ (Talbot and Arnett 1975)

$$H_g = \frac{\sigma_g^2}{\pi G \mu_g} \frac{1}{(1 + \beta/\alpha)}, \quad (9)$$

where the quantities α and β relate the vertical velocity dispersion σ_*^2 and surface mass density μ_* of the stars to those of the gas clouds

$$\sigma_* = \alpha \sigma_g, \quad (10a)$$

$$\mu_* = \beta \mu_g. \quad (10b)$$

2.3 Stability of a two-component rotating disc

The stability of rotating discs of gas and collisionless particles to axisymmetric modes has been analysed in classic papers by Goldreich and Lynden-Bell (1965) and by Toomre (1964). Here we use the results of Jog and Solomon (1984) who analysed the stability of a rotating disc consisting of two isothermal fluids of sound speeds c_1 , c_2 and surface mass densities μ_1 and μ_2 . These authors find that such a disc is stable to axisymmetric modes of wavenumber k if

$$x = \frac{2\pi G \mu_1}{\kappa^2} \frac{k}{(1 + k^2 c_1^2 / \kappa^2)} + \frac{2\pi G \mu_2}{\kappa^2} \frac{k}{(1 + k^2 c_2^2 / \kappa^2)} < 1, \quad (11)$$

where κ is the epicyclic frequency

$$\kappa = 2\omega \left(1 + \frac{1}{2} \frac{r}{\omega} \frac{d\omega}{dr}\right)^{1/2}. \quad (12)$$

Equation (11) yields a cubic equation for the most unstable mode k_m . Solving this equation in terms of the parameters α and β of equations (10), and ignoring the small differences between a gaseous and collisionless disc, we can write the stability criterion for a two-component system as

$$\sigma_g = \frac{\pi G \mu_g}{\kappa} g(\alpha, \beta). \quad (13)$$

This is identical to the Goldreich-Lynden-Bell criterion except for the factor $g(\alpha, \beta)$. This factor is plotted in Figure 1 for various values of α and β .

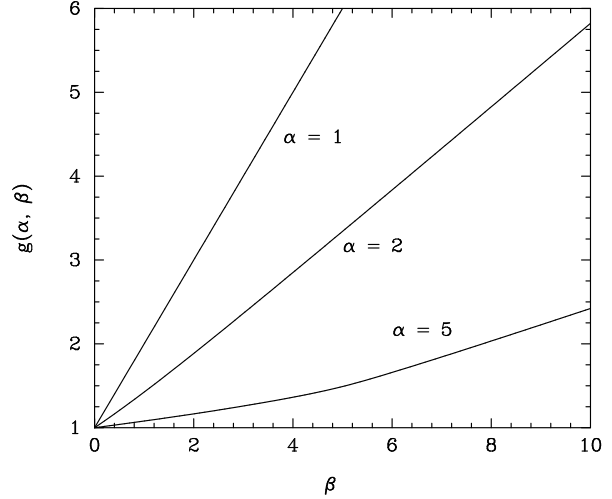


Figure 1. The factor $g(\alpha, \beta)$ appearing in the stability criterion of equation (13) plotted against β for three values of α

2.4 Star formation and supernovae energy input

We assume a stellar initial mass function (IMF) of the standard Salpeter (1955) form

$$\frac{dN_*}{dm} = A m^{-(1+x)}, \quad m_l < m < m_u, \quad x = 1.35, \quad (14)$$

$$m_l = 0.1 M_\odot, \quad m_u = 50 M_\odot,$$

and that each star of mass greater than $8 M_\odot$ releases $10^{51} E_{51}$ ergs in kinetic energy in a supernova explosion. For the IMF of equation (14), one supernova is formed for every $125 M_\odot$ of star formation. The energy injection rate is therefore related to the star formation rate by

$$\dot{E}_{sn} = 2.5 \times 10^{41} E_{51} \dot{M}_* \text{ erg/sec}, \quad (15)$$

where \dot{M}_* is the star formation rate in M_\odot per year.

2.5 Energy dissipated by cloud collisions

We assume cold clouds of constant density $\bar{\rho}_c = 7 \times 10^{-23} \text{ g/cm}^3$ with a distribution of cloud radii

$$\frac{dN_{ca}}{da} = N_0 a^{-4}, \quad a_l < a < a_u, \quad (16)$$

$$a_l = 0.5 \text{ pc}, \quad a_u = 10 \text{ pc},$$

(MO77). Following MO77, the clouds are assumed to have an isotropic Gaussian velocity distribution with velocity dispersion independent of cloud size and that they lose energy through inelastic collisions. The rate of energy loss per unit volume is given by

$$\frac{dE_{coll}}{dt dV} = 24\pi^{3/2} \bar{\rho}_c N_{cl}^2 a_l^5 \sigma_g^3 I_a, \quad (17)$$

$$I_a = \frac{1}{2} \int_1^{a_u/a_l} \int_1^{a_u/a_l} \frac{(x+y)^2}{(x^3+y^3)} \frac{dx dy}{x y},$$

where N_{cl} is the local cloud density $N_{cl} = N_0/3a_l^3$. Integrating equation (17) over the vertical direction and using equation (9) for the scale height, the rate of energy loss per

Table 1: Parameters of Model Galaxies

	v_c (km/s)	v_{\max} (km/s)	v_v/v_c	r_D (kpc)	M_D (M_\odot)	f_{coll}	c	λ_H
Model MW	280	212	0.45	3.0	5.5×10^{10}	50	10	0.065
Model DW	70	53	0.45	0.2	2.3×10^8	50	10	0.065

unit surface area $\dot{E}_{\text{coll}}^\Omega$ is

$$\dot{E}_{\text{coll}}^\Omega = 5.0 \times 10^{29} \left(1 + \frac{\beta}{\alpha}\right) \mu_{g5}^3 \sigma_{g5} \text{ erg/sec/pc}^2, \quad (18)$$

where μ_{g5} is the surface mass density of the gas component in units of $5M_\odot/\text{pc}^2$ and σ_{g5} is the cloud velocity dispersion in units of 5 km/sec. These values are close to those observed in the local solar neighbourhood. To estimate the efficiency with which supernovae accelerate the system of clouds, we normalize to the observed net star formation rate of the Milky Way. Assuming that the gas distribution has a flat surface mass density profile to $R_{\max} = 14$ kpc (Mihalas and Binney 1981), $\beta \approx 10$, $\alpha \approx 5$, and equating the integral of (18) to $\epsilon_c \dot{E}_{\text{sn}}$ (equation 15), we find

$$\epsilon_c E_{51} \dot{M}_* = 0.004. \quad (19)$$

An efficiency parameter of $\epsilon_c = 0.01$ produces a net star formation rate of $0.4M_\odot/\text{yr}$ which is reasonable for a Milky Way-like galaxy. We will therefore adopt a constant value of $\epsilon_c = 0.01$ in the models of the next subsection. The value of ϵ_c will, of course, depend on the properties of the clouds, ISM and star formation rate. For example, in the model of MO77 the clouds are accelerated by interactions with the cold shells surrounding supernova remnants and they find efficiencies ϵ_c of typically a few percent. We investigate the effect of varying ϵ_c in Section 6.

2.6 Self-regulating models without inflow or outflow

The equations derived above allow us to evolve an initially gaseous disc and to compute the local star formation rate, cloud velocity dispersion *etc.* The system of stars and gas is constrained to satisfy the stability criterion of equation (13), which fixes the cloud velocity dispersion σ_g . There is some empirical evidence that star formation in nearby galaxies is regulated by a stability criterion of this sort (*e.g.* Kennicutt 1998). The energy lost in cloud collisions (equation 18) is balanced against the energy input from supernovae assuming a constant efficiency factor $\epsilon_c = 0.01$. We assume further that $\alpha = 5$ (equation 10a) *i.e.* that stars are instantaneously accelerated to higher random velocities than the system of gas clouds, and that the properties of the gas clouds (mass spectrum, internal density, *etc.*) are independent of time. These are clearly restrictive assumptions, but they allow us to generate simple models of self-regulating star formation with only one free parameter ϵ_c .

We study the evolution of two model galaxies with parameters listed in Table 1. Model MW has parameters roughly similar to those of the Milky Way and model DW has parameters similar to those of a relatively high surface brightness dwarf galaxy.

Figure 2 shows the evolution of the gas and stellar surface mass densities of the two models. The net star formation rates, gas fractions and mean gas cloud velocity dispersion are plotted in Figure 3. In model MW, the star formation rates are initially high ($> 100M_\odot/\text{yr}$) and hence the timescale for star formation is short; half the disc mass is converted into stars in 10^7 years. The star formation rate declines rapidly to less than $1M_\odot/\text{yr}$ after a few Gyr. As figure 2 shows, the star formation at early times is concentrated to the inner parts of the disc which have a high surface density and hence the gas distribution develops a characteristic surface density profile with an inner ‘hole’, similar to what is seen in the HI distributions in real galaxies (see Burton 1991). The stellar disc is truncated at about the Holmberg (1958) radius ($r/r_D \approx 5$), in rough agreement with observations. The truncation arises because the gas disc becomes thick at large radii (equation 9) and the rate of energy lost in cloud collisions can be balanced by a very low star formation rate.

The evolution of model DW is qualitatively similar, though the star formation rate is scaled down roughly in proportion to the disc mass. Half the gas is converted to stars by 3×10^7 yr, and the gas fraction is 0.12 after 10^{10} yr, similar to the final gas fraction of 0.13 in model MW.

Neither of these models is satisfactory. The star formation rate in model MW is too high at early times to be compatible with deep number counts (see *e.g.* Ellis 1997), which require more gentle star formation rates in typical L^* galaxies. Model DW converts most of its gas into stars on a short timescale and so does not solve the problem raised in the introduction of explaining the flat faint end slope of the luminosity function in CDM-like models. As we will see in later sections, infall of gas provides the solution to the former problem, since this allows the disc to build up gradually on a cooling or dynamical timescale. Outflow of hot gas heated by supernovae provides a solution to the latter problem.

3 EVOLUTION OF A TWO-PHASE ISM

In this Section we consider the interaction of a multiphase interstellar medium with expanding supernova remnants following the model of MO77 and discuss the conditions under which a protogalaxy can form a wind. The key ingredients of the model are as follows. Most of the cold gaseous mass is assumed to be in cold clouds with properties as given in Section 2.5. Supernovae explode and their remnants propagate evaporating some of the cold clouds and forming a low density hot phase of the ISM. The star formation rate therefore determines the evaporation rate and hence the rate of conversion of the cold phase to a hot phase. A wind from the galaxy can result if the hot phase is: (i) sufficiently pervasive

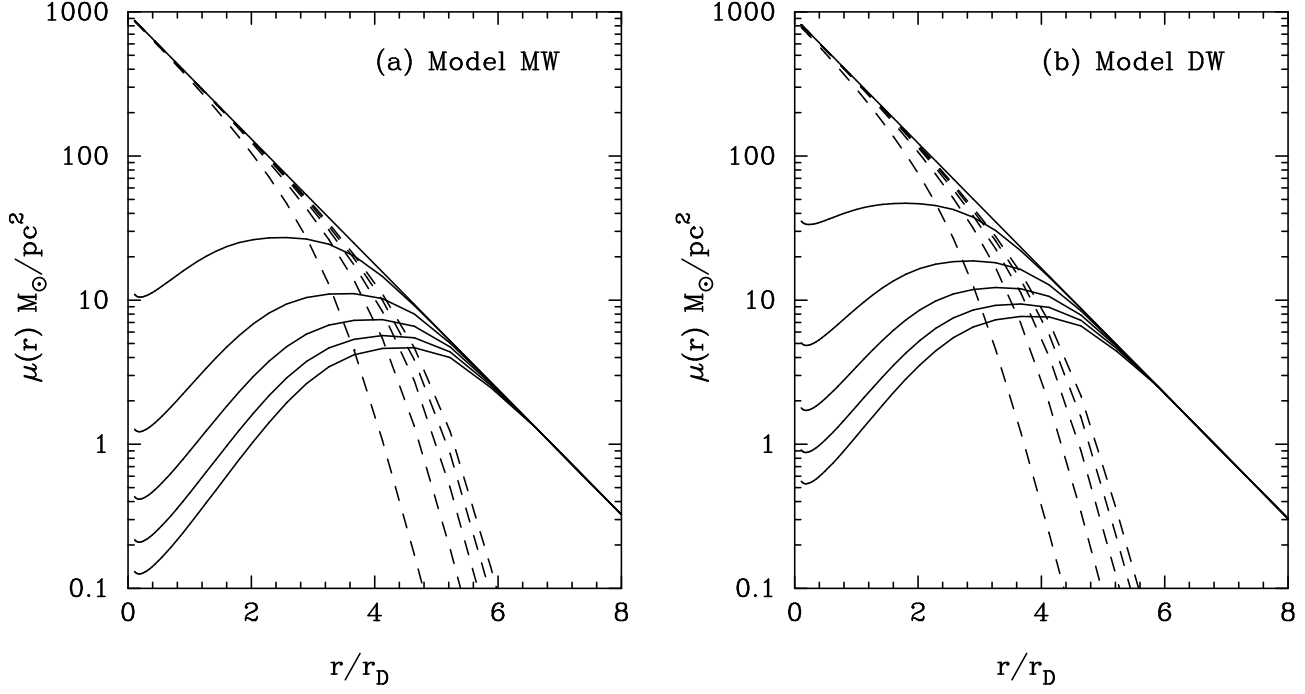


Figure 2. The evolution of the gas (solid lines) and stellar (dashed lines) surface mass density distributions according to the simple self-regulating model described in this section. The results are shown for ages of 0, 0.1, 1, 3, 6 and 10 Gyr.

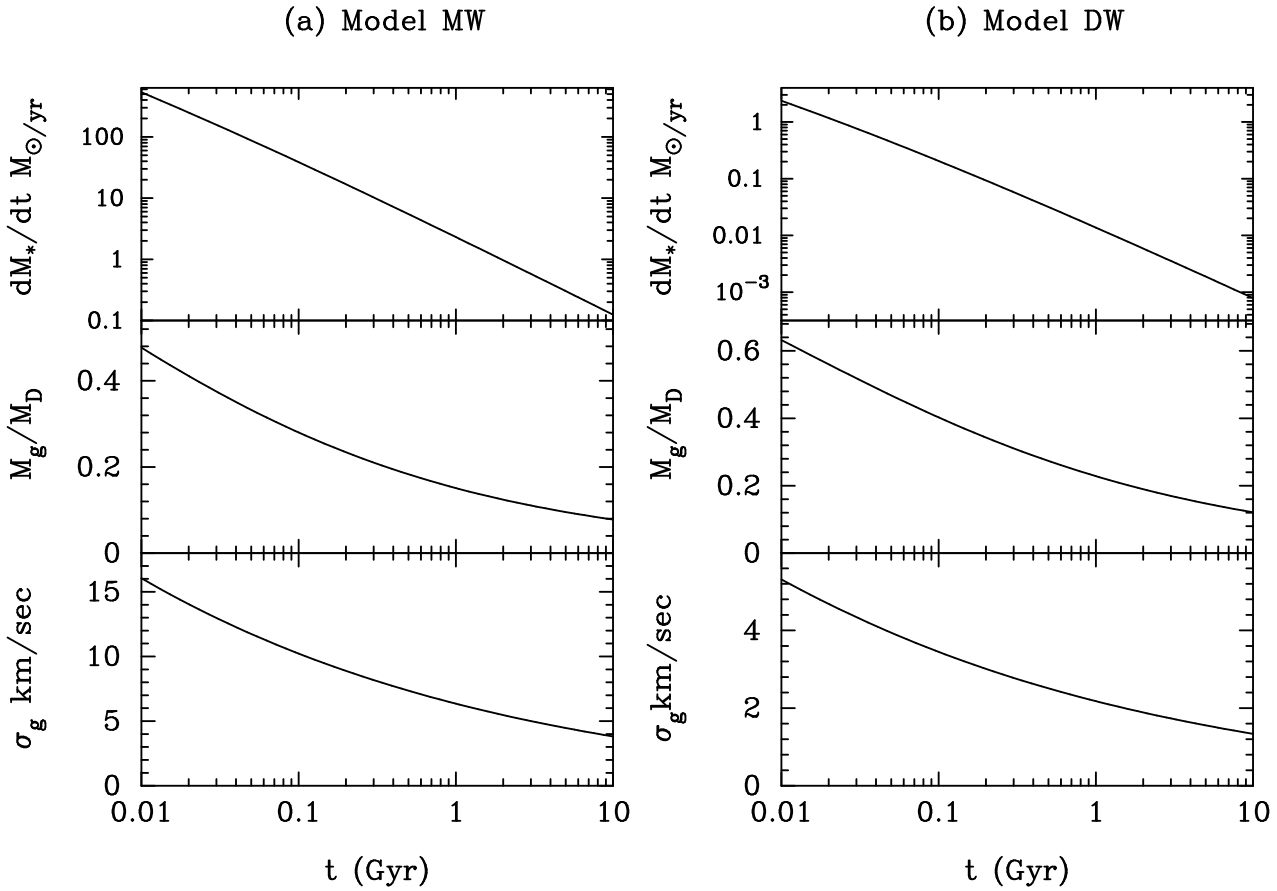


Figure 3. Evolution of the star formation rate, gas fraction and gas cloud velocity dispersion in the self-regulating model.

(filling factor of order unity), (ii) low density (so that radiative cooling is unimportant) and (iii) the temperature of the hot phase exceeds the virial temperature of the galaxy. In this section we follow closely the theory of the ISM developed by MO77 and we use their notation where possible.

3.1 Evaporation of cold clouds

An expanding supernovae remnant will evaporate a mass of

$$M_{ev} \approx 540 E_{51}^{6/5} \Sigma^{-3/5} n_h^{-4/5} M_{\odot}, \quad (20)$$

where n_h is the density interior to the supernovae remnant and Σ (in pc^2) is the evaporation parameter introduced by MO77

$$\Sigma = \frac{\gamma}{4\pi a_l N_{cl} \phi_{\kappa}}. \quad (21)$$

Here the parameter γ relates the blast wave velocity to the isothermal sound speed ($v_b = \gamma c_h$, $\gamma \approx 2.5$) and the parameter ϕ_{κ} quantifies the effectiveness of the classical thermal conductivity of the clouds ($\kappa_{eff} = \kappa \phi_{\kappa}$) and so is less than unity if the conductivity is reduced by tangled magnetic fields, turbulence *etc.* Using equations (7) and (9) to estimate the mean cloud density we find

$$\Sigma \approx 280 \frac{\sigma_{g5}^2}{\mu_{g5}^2} \frac{1}{(1 + \beta/\alpha)} \frac{1}{\phi_{\kappa}} \text{pc}^2 = f_{\Sigma} \Sigma_{\odot}, \quad \Sigma_{\odot} \approx 95 \text{pc}^2, \quad (22)$$

where Σ_{\odot} is the evaporation parameter characteristic of the local solar neighbourhood ($\beta/\alpha \approx 2$).

Evaluating equation (20), we find

$$M_{ev} \approx 1390 E_{51}^{6/5} f_{\Sigma}^{-3/5} \phi_{\kappa}^{3/5} n_{h-2}^{-4/5} M_{\odot}, \quad (23)$$

where n_{h-2} is n_h in units of 10^{-2}cm^{-2} (a characteristic value for the hot component). Thus, provided thermal conduction is not highly suppressed, a single supernovae remnant can evaporate a much larger mass than the $125 M_{\odot}$ formed in stars per supernovae for a standard Salpeter IMF (Section 2.4). If a significant fraction of this evaporated gas can escape in a wind, then star formation will be efficiently suppressed.

3.2 Temperature and density of the hot phase

To compute the properties of the hot phase we assume that the disc achieves a state in which the porosity parameter Q is equal to unity. The disc is then permeated by a network of overlapping supernovae remnants. Ignoring cooling interior to the remnants (which we will see is a reasonable approximation for an ISM with low metallicity) the age, radius and temperature of a SNR when $Q = 1$ are given by

$$t_o = 5.5 \times 10^6 S_{13}^{-5/11} \gamma^{-6/11} E_{51}^{-3/11} n_h^{3/11} \text{yr}, \quad (24a)$$

$$R_o = 100 S_{13}^{-2/11} \gamma^{2/11} E_{51}^{1/11} n_h^{-1/11} \text{pc}, \quad (24b)$$

$$T_o = 1.2 \times 10^4 S_{13}^{6/11} \gamma^{-6/11} E_{51}^{8/11} n_h^{-8/11} \text{K}. \quad (24c)$$

where S_{13} is the supernova rate in units of $10^{-13} \text{pc}^{-3} \text{yr}^{-1}$. The density of a remnant at t_o ($n_h^o \approx M_{ev}/(4/3\pi R_o^3)$), gives an approximate estimate of the density of the ambient hot phase

$$n_h^o \approx 4.3 \times 10^{-3} S_{13}^{0.36} \gamma^{-0.36} E_{51}^{0.61} f_{\Sigma}^{-0.393} \text{cm}^{-3}. \quad (25)$$

Inserting this estimate into equations (24) we find

$$t_o = 1.2 \times 10^6 S_{13}^{-0.36} \gamma^{-0.64} (E_{51} f_{\Sigma})^{-0.11} \text{yr}, \quad (26a)$$

$$R_o = 164 (S_{13}/\gamma)^{-0.21} E_{51}^{0.04} f_{\Sigma}^{0.035} \text{pc}, \quad (26b)$$

$$T_o = 6.6 \times 10^5 (S_{13} E_{51} f_{\Sigma}/\gamma)^{0.29} \text{K}, \quad (26c)$$

and the rate at which clouds are evaporated is

$$\dot{M}_{ev} = 2.7 \times 10^{-10} S_{13}^{0.71} \gamma^{0.29} E_{51}^{0.71} f_{\Sigma}^{-0.29} M_{\odot} \text{pc}^{-3} \text{yr}^{-1}. \quad (27)$$

Integrating equation (27) over the scale height of the disc gives the evaporated mass per unit area,

$$\dot{M}_{ev}^{\Omega} \approx 1 \times 10^{-7} \left(\frac{\sigma_{g5}^2}{\mu_{g5} (1 + \beta/\alpha)} \right) \times S_{13}^{0.71} \gamma^{0.29} E_{51}^{0.71} f_{\Sigma}^{-0.29} M_{\odot} \text{pc}^{-2} \text{yr}^{-1}. \quad (28)$$

Adopting a cooling rate of $\Lambda \approx 2.5 \times 10^{-22} T_5^{-1.4} \text{erg cm}^3 \text{s}^{-1}$ for $10^5 \lesssim T \lesssim 10^6$ for a gas with primordial composition, the ratio of t_o to the cooling time t_{cool} is

$$\frac{t_o}{t_{cool}} \approx 0.5 T_5^{-2.4} f_{\Sigma}^{-0.5}, \quad (29)$$

Thus if the temperature of the hot phase is higher than about 10^5K , the assumption that cooling can be neglected will be valid. A cooling function for a gas with primordial composition will be used throughout this paper. As the metallicity of the gas builds up, the cooling time of the hot component will shorten and more of the supernovae energy will be lost radiatively. This effect will reduce the efficiency of feedback in galaxies with high metallicity but is not included in this paper.

3.3 Simple self-regulating model with outflow

In this section we apply the results of the previous paragraphs to construct a simplified self-regulating model with outflow. The star formation rate is governed by the self-regulation algorithm as in Section 2.6 with the parameter $\epsilon_c = 0.01$. This provides an estimate of the local supernova rate per unit volume which we insert in equations (26) to compute the properties of the hot phase, adopting a value $\phi_{\kappa} = 0.1$ in equation (21) for the conduction efficiency parameter. The hot gas will be lost from the system if its specific enthalpy

$$\frac{1}{2} v^2 + \frac{5p}{\rho}$$

exceeds to within a factor of order unity its gravitational binding energy per unit mass. If the gas has an initial isothermal sound speed of $c_i = (kT/\mu_p) = 37 T_5^{1/2} \text{kms}^{-1}$ (for a mean mass per particle of $\mu_p = 0.61 m_p$), conservation of specific enthalpy implies that the wind will reach a bulk speed of $v_w \approx \sqrt{5} c_i$. Some of the thermal energy will be lost radiatively, and in fact the spherical steady wind solutions described in Appendix B suggest that a more accurate criterion for the wind to escape from a galaxy is $v_w \approx \sqrt{2.5} c_i > v_{esc}$, where v_{esc} is the escape speed from the centre of the halo (neglecting the potential of the disc). If $\sqrt{2.5} c_i < v_{esc}$, the hot phase is returned instantaneously to the cold phase. This type of binding energy criterion for outflow has been adopted in previous studies (*e.g.* Larson 1974, Dekel and Silk 1986) and is clearly oversimplified, as are the assumptions of instantaneous mass loss and return

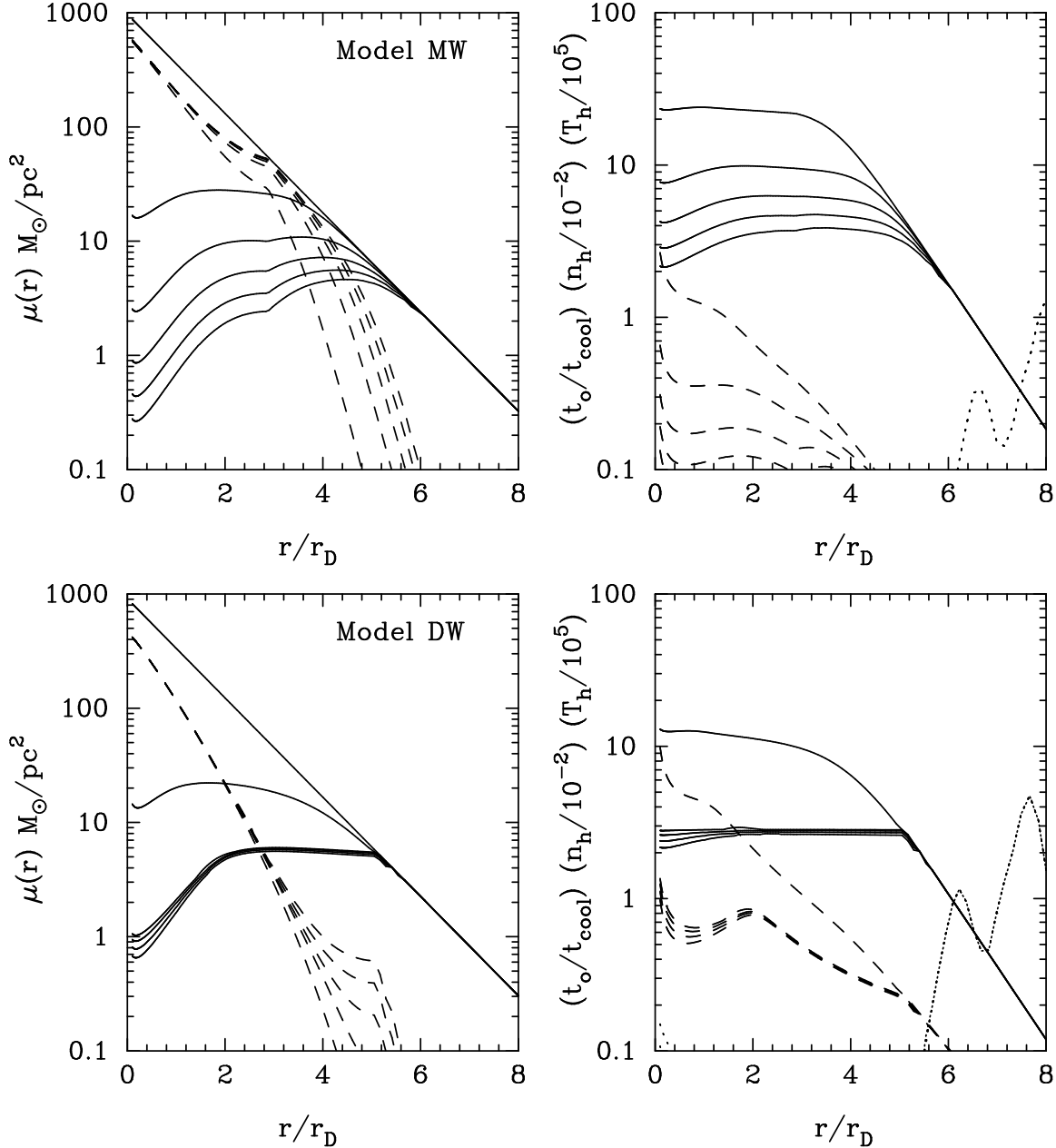


Figure 4. The left hand panels show the evolution of the gas (solid lines) and stellar (dashed lines) surface mass density distributions for ages of 0, 0.1, 1, 3, 6 and 10 Gyr as in figure 2. The panels to the right show various properties of the hot gas component as a function of the disc radius r/r_D . The solid lines show the temperature, dashed lines show the density and the dotted lines show the ratio of overlap to cooling timescales, t_o/t_{cool} .

of cold gas. These points will be discussed further in Section 6, but for the moment these assumptions will be adopted to illustrate the qualitative features of the model. As gas is lost from the system, the circular speed of the disc component (equation 5) is simply rescaled by the square root of the mass of the disc that remains.

The evolution of the surface mass densities for the two disc models is illustrated in Figures 4 and 5. In model MW, the evolution is similar to that without outflow shown in Figure 2. With the simple prescription for mass loss used

here, no hot gas is lost unless the temperature of the hot phase exceeds $T_{\text{crit}} \approx 5 \times 10^6 \text{K}$. This does happen at early times when the star formation rate is high, and about 25% of the galaxy mass is lost within 10^7 yr. Thereafter, no more mass is lost and a nearly exponential disc is built up with a gas distribution containing a central hole as in Figure 2. The star formation rate in this model declines strongly with time, exceeding $100 M_{\odot}/\text{yr}$ in the early phases of evolution.

The behaviour of model DW is qualitatively different. Here the critical temperature for mass loss is much lower,

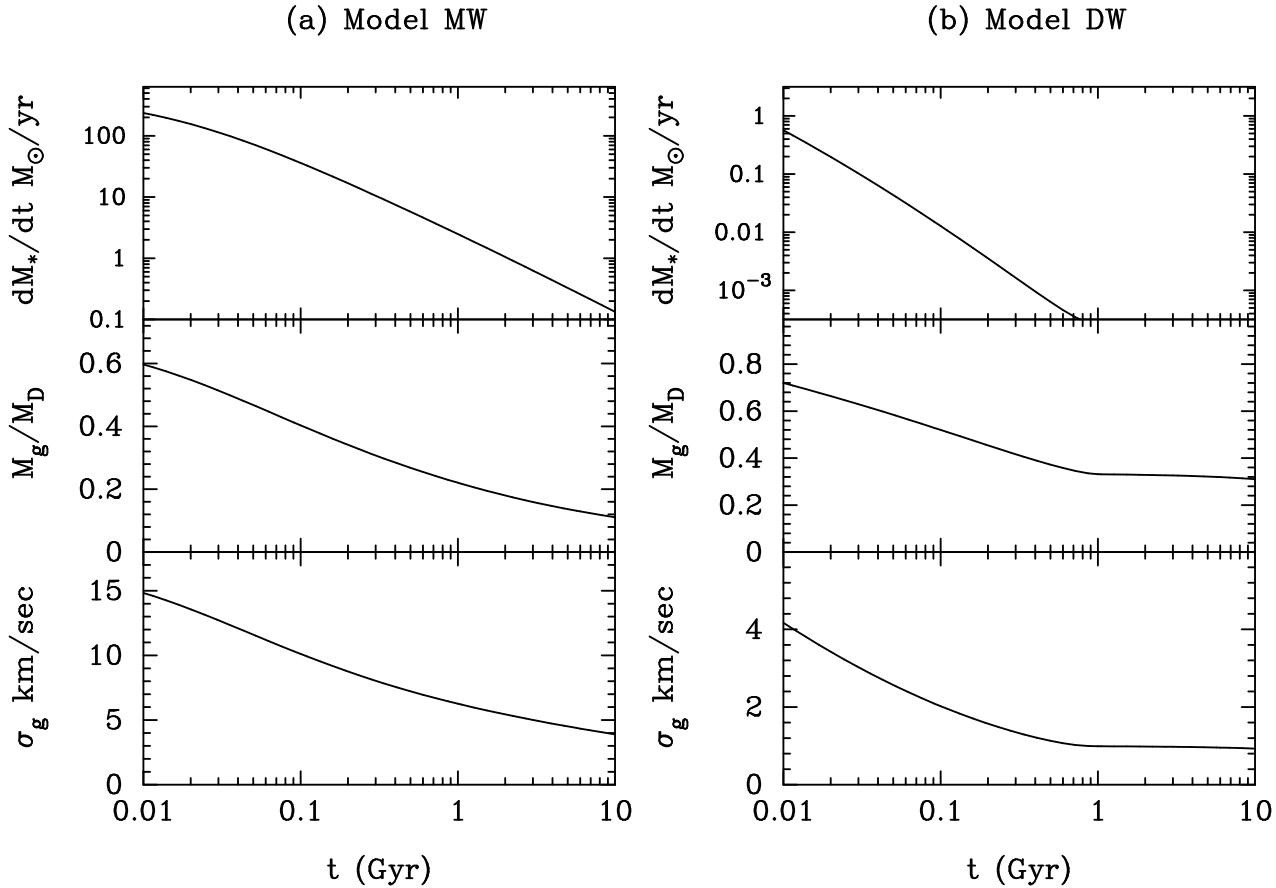


Figure 5. Evolution of the star formation rate, gas fraction and gas cloud velocity dispersion for the models shown in figure 4.

$T_{crit} \approx 3 \times 10^5$ K, hence half the mass of the galaxy is expelled by $\sim 10^8$ yr and 66% by 1 Gyr. After 1 Gyr, the temperature of the hot phase drops below T_{crit} and the galaxy settles into a stable state with a low rate of star formation.

The wind prescription in these models, and particularly the assumption that gas below the critical temperature necessary for escape is returned instantaneously to the cold phase, is clearly oversimplified and so the mass loss fractions should not be taken too seriously. A more detailed model is developed in Section 6. A more serious deficiency of the model presented here is that the entire gas disc is assumed to have formed instantaneously at $t = 0$. This is unrealistic and leads to high rates of star formation and gas ejection at early times. A simple infall model, similar to those adopted in semi-analytic models (White and Frenk 1991, Cole *et al.* 1994) is included in the next Section.

4 INFALL MODEL

4.1 Conservation of specific angular momentum

Following Fall and Efstathiou (1980), the gas is assumed to follow the spatial distribution of the halo component with the same distribution of specific angular momentum prior to collapse. The halo is assumed to rotate cylindrically with rotation speed $v_H^{rot}(\varpi_H)$, where ϖ_H is the radial coordinate

in the cylindrical coordinate system. The gas is assumed to conserve its specific angular momentum during its collapse, so that the final specific angular momentum of the disc at radius ϖ_D , $h_D = \varpi_D v_D^{rot}$, is equal to the specific angular momentum of the halo $h_D = \varpi_H v_H^{rot}$ at the radius ϖ_H from which the gas originated. Mass conservation relates the radii ϖ_H and ϖ_D ,

$$\frac{d\varpi_H}{d\varpi_D} = \frac{\mu_D(\varpi_D)}{\mu_H(\varpi_H)} \frac{M_H}{M_D} \frac{\varpi_D}{\varpi_H}, \quad (30)$$

where M_H/M_D is the ratio of the halo to disc mass interior to the maximum infall radius of the disc (see figure 6a below) and μ_H is the projected surface mass density of the halo

$$\mu_H(\varpi) = 2 \int_0^\infty \rho_H ((\varpi^2 + z^2)^{1/2}) dz. \quad (31)$$

The solution of equation (30) yields $\varpi_D(\varpi_H)$ and the rotation speed of the halo follows from the conservation of specific angular momentum, $v_H^{rot} = \varpi_D v_D^{rot}(\varpi_D)/\varpi_H$. The results for the parameters of models MW and DW are shown in figure 6, where we have used the notation $s = \varpi/r_D$. When expressed in the dimensionless units of Figure 6, the solutions for models MW and DW are identical.

This prescription is guaranteed to form an exponential disc with the required parameters. The derived rotation velocity of the halo is almost independent of radius in general agreement with what is found in N-body simulations (Frenk

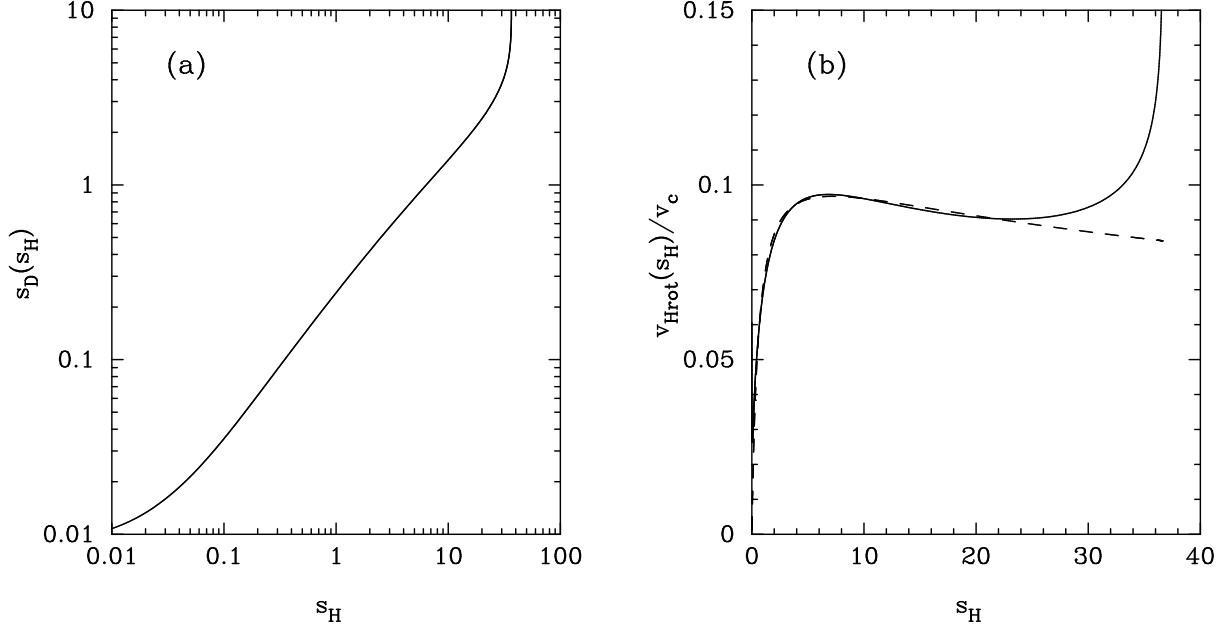


Figure 6. Figure 6a shows the solution of the mass conservation equation (30) relating the initial halo radius $s_H = \varpi_H/r_D$ to the final disc radius $s_D = \varpi_D/r_D$. The solid line in figure 6b shows the derived rotation curve of the halo in units of $v_c = (GM_D/r_D)^{1/2}$ assuming conservation of specific angular momentum $h_H = h_D$. The dashed line shows the fitting function of equation (39).

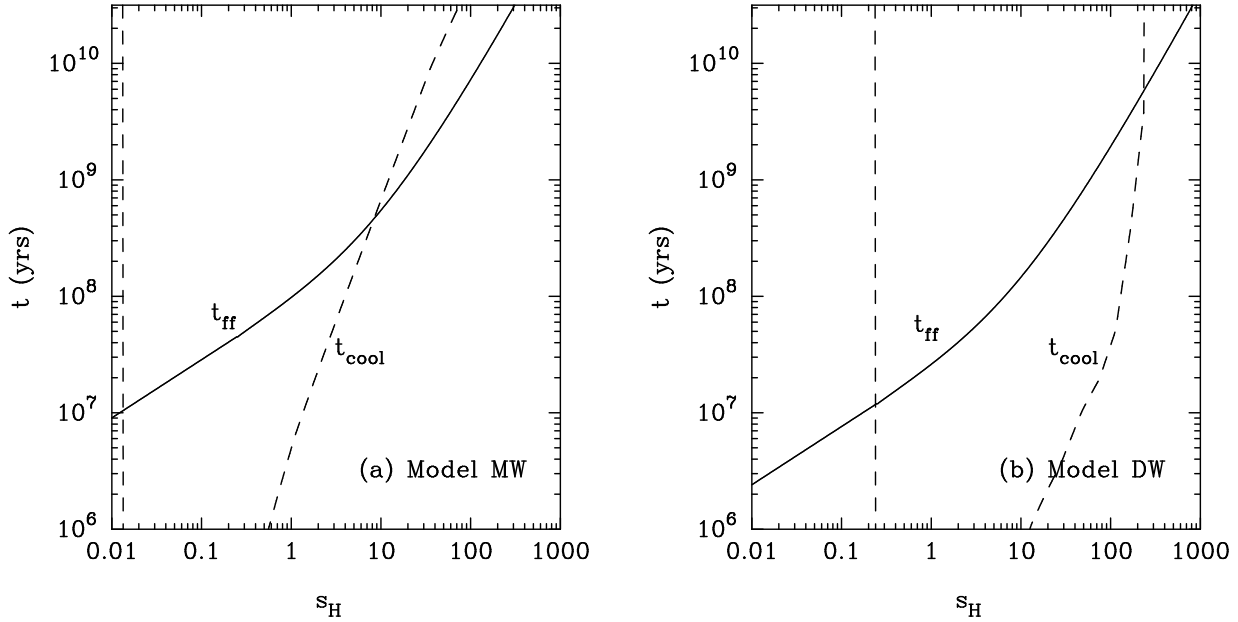


Figure 7. The free-fall (solid lines) and cooling times (dashed lines) for the two model galaxies plotted as a function of halo radius r_H/r_D . Note that for these models, the ratio of baryonic to dark mass within the virial radius is 0.1.

et al. 1988, Warren *et al.* 1992). The upturn in the halo rotation speed at $s_H(\text{max}) \approx 30$ is caused by the rapid decline in the mass of the input exponential disc at large radii and is of little consequence in the discussion that follows. The values of the spin parameter quoted in Table 1 were derived from the mass and binding energy of the halo and assuming

that the the halo rotation velocity is constant at $0.095v_c$ at large radii.

4.2 Mass infall rate

To determine the gas infall rate we compute the free fall time for a gas element at rest at radius r_i ,

$$t_{\text{ff}} = \int_0^{r_i} \frac{dr}{\sqrt{2[\phi_H(r_i) - \phi_H(r)]^{1/2}}}, \quad (32)$$

and the cooling time

$$t_{\text{cool}} = \frac{3 kT_v \times 1.92}{2 \Lambda(T_v) n_e(r)}, \quad (33)$$

where $n_e(r)$ is the electron density. The temperature T_v in equation (33) is set to the virial temperature derived from the equation of hydrostatic equilibrium assuming that the temperature is slowly varying with radius

$$T_v \approx -v_H^2(r) \frac{\mu_p}{k} \frac{d \ln r}{d \ln \rho_b(r)}, \quad (34)$$

where we assume that the baryons follow the same spatial distribution as the halo. The infall rate is given by

$$\dot{M}_{\text{inf}} = 4\pi \rho_b(r_H) r_H^2 \begin{cases} dr_H(t_{\text{ff}} = t)/dt & t_{\text{ff}} > t_{\text{cool}} \\ dr_H(t_{\text{cool}} = t)/dt & t_{\text{cool}} > t_{\text{ff}} \end{cases}. \quad (35)$$

Finally, conservation of specific angular momentum specifies the final radius in the disc for each gas element. Since the halo is assumed to rotate on cylinders, the gas near to the poles in an infalling shell has a lower specific angular momentum than the gas at the equator. The infalling material is therefore distributed through the disc according to

$$2\pi \varpi_D \dot{\mu}_D(\varpi_D) d\varpi_D = \dot{M}_{\text{inf}} \frac{\varpi_H d\varpi_H}{r_H (r_H^2 - \varpi_H^2)^{1/2}}, \quad (36)$$

where ϖ_D and ϖ_H are related by the solution of equation (30).

Equations (32) – (36) specify the infall model. The free-fall and cooling times of the two model galaxies are shown in Figure 7. In the larger galaxy, gas within $r_H/r_D \approx 10$ infalls on the free-fall timescale and ends up within one scale length of the final disc. The material in the outer parts of the disc infalls on the cooling timescale. In contrast, apart from a small amount of gas in the very central part of the halo with virial temperature $< 10^4$ K, the gas in the dwarf galaxy infalls on a free-fall timescale because the cooling time is so short.

4.3 Simple self-regulating model with inflow and outflow

The models described in this section are exactly the same as those described in section 3.3, except that we grow the discs gradually using the infall model of sections 4.1 and 4.2. In the models described below, inflow and outflow are assumed to occur simultaneously. This is often assumed in semi-analytic models of galaxy formation (*e.g.* Cole *et al.* 1994, Somerville and Primack 1999) and may not be completely unrealistic if the infalling gas is clumpy. The dark matter haloes will contain significant sub-structure (*e.g.* Moore *et al.* 1999) which may contain pockets of cooled gas. Furthermore, if the cooling time is short compared to the dynamical time, the infalling gas will be thermally unstable (Fall and Rees 1985) and will fragment into clouds. These will fall to the centre on a free-fall timescale if they

are sufficiently dense and massive that gravity dominates over the ram pressure of the wind. This requires clouds with masses

$$m_{\text{cloud}} \gtrsim 9.5 \times 10^5 M_{\odot} \left(\frac{a_{\text{cloud}}}{1 \text{ kpc}} \right) \left(\frac{r}{10 \text{ kpc}} \right)^{-1} \times \left(\frac{\dot{M}_w}{1 M_{\odot}/\text{yr}} \right) \left(\frac{v_w}{100 \text{ km/s}} \right) \left(\frac{v_v}{100 \text{ km/s}} \right)^{-2}, \quad (37)$$

where a_{cloud} is the radius of the cloud. However, even if (37) is satisfied, the clouds may be sheared and disrupted into smaller clouds by Kelvin-Helmholtz instabilities on a timescale of a few sound crossing times as they flow through the wind (*e.g.* Murray *et al.* 1993). The wind energy will be partially thermalized in shocks with the infalling clouds and dissipated in evaporating small clouds. But for the typical mass outflow rates expected from dwarf galaxies ($\dot{M}_w \lesssim 0.2 M_{\odot}/\text{yr}$), the rate at which energy is supplied by the wind $\dot{E}_w = 1/2 \dot{M}_w v_w^2$ is much smaller than the energy lost in radiative cooling,

$$\frac{\dot{E}_{\text{cool}}}{\dot{E}_w} \approx 50 \Lambda_{-23} \left(\frac{v_v}{100 \text{ km/s}} \right)^4 \left(\frac{r_{\text{cool}}}{10 \text{ kpc}} \right)^{-1} \times \left(\frac{v_w}{100 \text{ km/s}} \right)^{-2} \left(\frac{\dot{M}_w}{1 M_{\odot}/\text{yr}} \right)^{-1}, \quad (38)$$

where r_{cool} is the radius at which the cooling time is equal to the age of the system.

The qualitative picture that we propose is as follows. In galaxies with a short cooling time, clouds formed by thermal instabilities will infall ballistically if (37) is satisfied. If (37) is not satisfied, the ram pressure of the wind will drive out the infalling gas and infall will be suppressed. With infall suppressed, the star formation rate in the disc and the wind energy will decline until infall can begin again. The wind will be partially thermalised before reaching r_{cool} and completely thermalised at $\sim r_{\text{cool}}$, but the energy supplied by the wind will be small compared to the energy radiated by the gas at $r \gtrsim r_{\text{cool}}$ and so cannot prevent radiative cooling. If (37) is satisfied, some of the outflowing gas may fall back down to the disc after shocking against infalling clouds. However, in the models described here the efficiency of converting infalling gas into stars is low in dwarf systems, so provided the gas does not cycle around the halo many times, neglecting return of some of the outflowing gas should not affect the qualitative features of the models. The global geometry of the system, *e.g.* if the wind is weakly collimated perpendicular to the disc, may also permit simultaneous inflow and outflow of gas.

The interaction of an outflowing wind with an inhomogeneous infalling gas clearly poses a complex physical problem. In reality, the process may be far from steady, with outflow occurring in bursts accompanied by infall from discrete sub-clumps containing cooled gas. In the models described below and in the rest of this paper, we will assume that the infall and outflow occur simultaneously, steadily and without any interaction between the inflowing and outflowing gas. As the discussion of the preceding two paragraphs indicates, this is obviously an over-simplification. It should be viewed as an idealization, on a similar footing to some of the other assumptions adopted in this paper (*e.g.* spherical symmetry, neglect of halo substructure and merging, steady

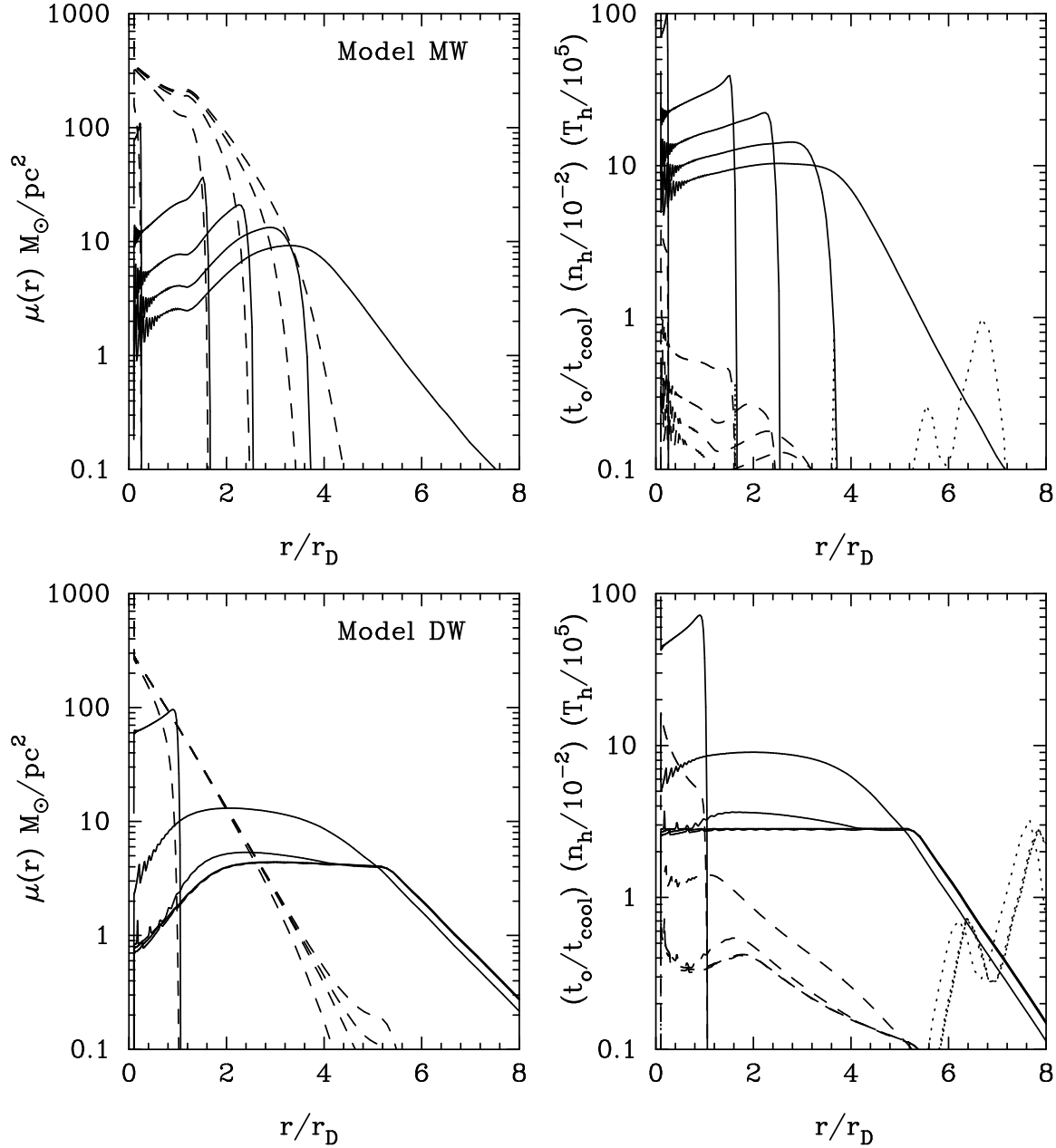


Figure 8. The left hand panels show the evolution of the gas (solid lines) and stellar (dashed lines) surface mass density distributions for ages of 0, 0.1, 1, 3, 6 and 10 Gyr as in figure 2. The panels to the right show the radial distribution of density, temperature and ratio of overlap to cooling timescales for the hot gas component.

star formation rates *etc*) designed to give some insight into how a quiescent mode of feedback might operate.

The analogues of figures 4 and 5 for the models incorporating infall and outflow are shown in figures 8 and 9. The discs build up from the inside out, as in the models of disc formation described by Fall and Efstathiou (1980) and Gunn (1982). Most of the star formation occurs in a propagating ring containing the most recently accreted gas. The most significant differences from the models of section 3.3, are the net rates of star formation (figure 9) and the timescale of outflow. The initial high rates of star formation in the models of section 3.3 are suppressed in the models with infall, and the timescale for outflow is now much longer because it

is closely linked to the gas infall timescale. Apart from these differences, the final states, gas fractions and mass-loss fractions are similar to those in the models without infall. In model MW some outflow occurs when $t \lesssim 10^8$ yrs and the temperature of the hot gas is high enough that it can escape from the system. Thereafter, the hot component cannot escape and the disc builds up without further outflow. About 17% of the total galaxy mass is expelled in the early phases of evolution, but as we have described above, this could be an overestimate since some of this gas may be returned to the galaxy if the wind energy is thermalized before it reaches the virial radius. In contrast, model DW drives a wind until $t \sim 1$ Gyr and expels about 74% of its mass. About half of

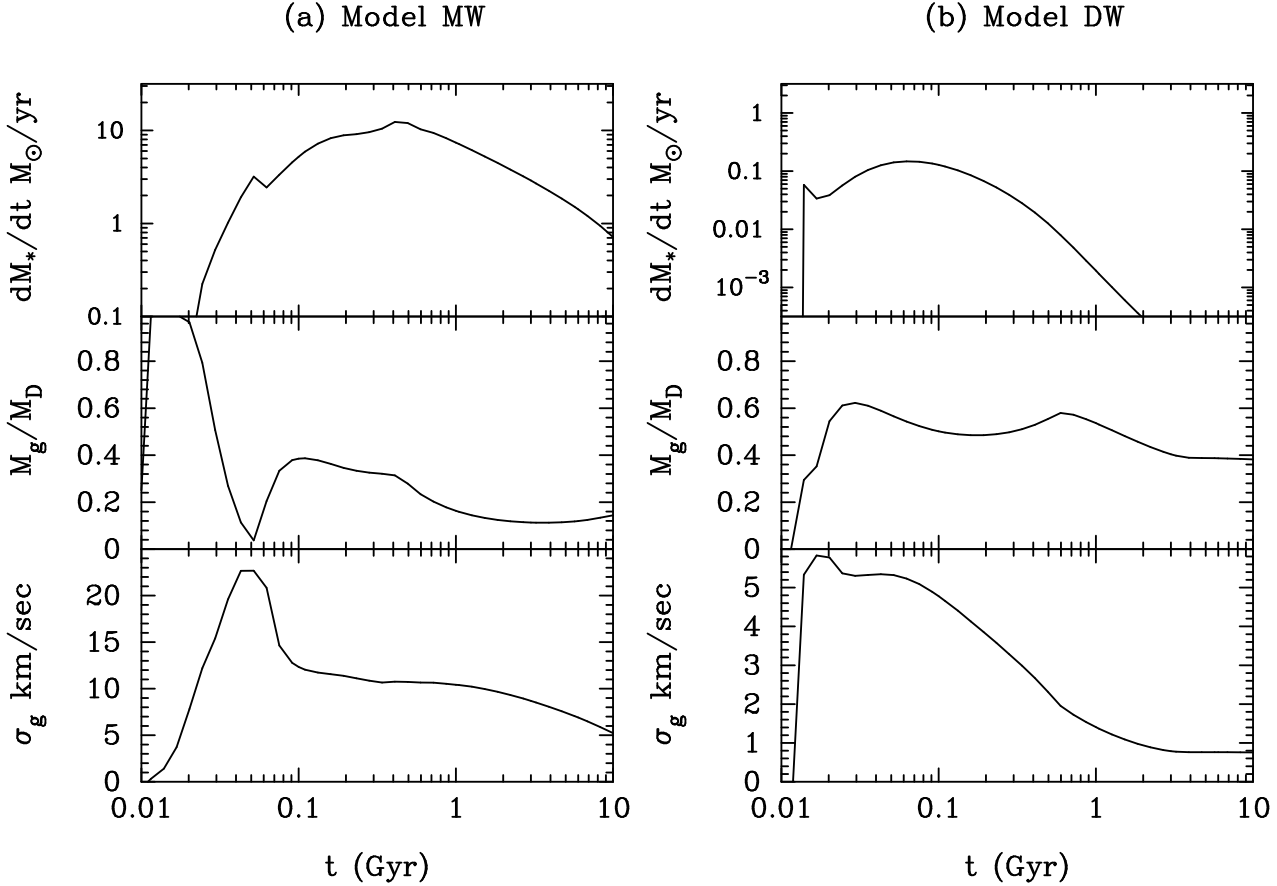


Figure 9. Evolution of the star formation rate, gas fraction and gas cloud velocity dispersion for the models shown in figure 8.

the gas is lost within 3×10^8 yrs, *i.e.* on about the infall timescale for most of the gas in the halo (see figure 7b).

5 REFINEMENTS OF THE MODEL

The models described in the previous sections contain a number of simplifications, which we will attempt to refine in this section. We do not address the problem of the interaction of a wind with the infalling gas, which is well beyond the scope of this paper. Instead, we introduce some simple improvements to the infall model (§5.1), model for mass loss from the galactic disc (§5.2, §5.3) and the pressure response of the cold ISM to the hot phase (§5.4, §5.5).

5.1 Infall Model

In Section 4, we used a simplified model of infall that guarantees the formation of an exponential disc if angular momentum is conserved during collapse. In this section, we assume a specific functional form for the rotation velocity of the halo,

$$v_H^{rot}(s) = c_1 v_c \frac{(s/c_2)}{(1 + (s/c_2))(1 + (s/c_3)^{c_4})}, \quad s \equiv r/r_D \quad (39)$$

with $c_1 = 0.115$, $c_2 = 0.6$, $c_3 = 16$, $c_4 = 0.25$. The functional form and coefficients in equation (39) have been chosen to provide a good fit to the halo rotation profile derived in section 4.1 from conservation of specific angular momentum

and is plotted as the dashed line in figure (6b). As in the previous section, the gas is assumed to follow the same radial density distribution and rotation velocity as the halo component, but its final radius in the disc is computed by assuming conservation of specific angular momentum and self-consistently solving for the rotation speed of the disc component. The halo component is assumed to be rigid and the contribution of the disc component to v_D^{rot} is computed using the Fourier-Bessel theorem (see Binney and Tremaine 1987 §2.6)

$$v^2(r) = -r \int_0^\infty S(k) J_1(kr) k dk, \\ S(k) = -2\pi G \int_0^\infty J_0(kr) \mu_D(r) r dr. \quad (40)$$

Equation (40) is time consuming to evaluate accurately and in our application $v^2(r)$ must be computed many times. A fast algorithm has therefore been developed as described in Appendix A. The epicyclic frequency κ is required in equation (13) to compute the instantaneous star formation rate and is derived by numerically differentiating the rotation speed.

With this formulation of the infall model, the infall rate is governed by the dark matter profile and the ratio of dark to baryonic mass within the virial radius, $M_v/M_D = (v_v/v_c)^2 f_{coll}$. For the models described here, we adopt $M_v/M_D = 10$, consistent with the parameters listed in Table 1. The final disc surface mass density will be close to an exponential by construction, since the halo rotation

velocity (39) has been chosen to match the rotation profile derived by assuming an exponential disc and conservation of specific angular momentum.

5.2 Galactic Fountain

In previous sections, we have assumed that gas is lost from the disc if the bulk velocity of the wind $v_w \approx \sqrt{2.5}c_i$, exceeds the escape speed v_{esc} from the halo, but is otherwise returned instantaneously to the ISM. More realistically, gas with $v_w < v_{esc}$ will circulate in the halo along a roughly ballistic trajectory and will cool forming a galactic fountain (Shapiro and Field 1976, Bregman 1980). In the models described in this section, hot gas with $v_w < v_{esc}$ is returned to the disc at the radius from which it was expelled after a time t_{ret} ,

$$t_{ret} = 2t_{ff}(r_{max}), \quad v_w^2 = 2[\phi_H(r_{max}) - \phi_H(0)], \quad (41)$$

i.e. we ignore the gravity of the disc and the angular momentum of the gas in computing the ballistic trajectory of a gas element.

5.3 Escape Velocity of the Wind

The detailed dynamics of the hot corona itself is complicated and beyond the scope of this paper. Type II supernovae at the upper and lower edges of the gas disc will be able to inject their energy directly into the hot gas, as will Type Ia supernovae forming in the thicker stellar disc. In addition, the hot component will interact with the primordial infalling gas in a complicated way as sketched in §4.3.

In the absence of radiative cooling, the hot gas will extend high above the galactic disc in an extended corona. For an isothermal corona, the equation of hydrostatic equilibrium in the z -direction has the following approximate solution,

$$\frac{\rho_H(\varpi, z)}{\rho_H(0)} \approx \text{sech}^{2p_g} \left(\frac{z}{H_g} \right) \text{sech}^{2p_s} \left(\frac{z}{H_s} \right) \times \exp \left(-\frac{1}{c_i^2} \int_0^z \frac{z v_H^2(r)}{r^2} dz \right), \quad r^2 = \varpi^2 + z^2, \quad (42)$$

$$p_g = \frac{\mu_g \sigma_g^2 \sigma_s}{c_i^2 (\mu_g \sigma_s + \mu_s \sigma_g)}, \quad p_s = \frac{\mu_s \sigma_s^2 \sigma_g}{c_i^2 (\mu_g \sigma_s + \mu_s \sigma_g)},$$

where we have assumed that both the stars and the gas follow sech^2 vertical distributions (equation 7) and c_i is the isothermal sound speed of the hot gas. We define a characteristic scale height for the hot component, $H_{hot}(\varpi)$, at which the density drops by a factor $\sim e$ according to equation (42). If radiative cooling were negligible, we would expect a sonic point in the flow at about $z \sim H_{hot}$. It is interesting to compare some characteristic numbers for the coronal gas:

$$\dot{E}_{in} \approx 1.1 \times 10^{40} T_{h6} \dot{M}_{ev} \text{ erg s}^{-1} \quad (43a)$$

$$\dot{E}_{SNII} \approx 5.7 \times 10^{40} \epsilon_{SNII} E_{51} \dot{M}_* \text{ erg s}^{-1} \quad (43b)$$

$$\dot{E}_{cool} \approx 2 \times 10^{39} n_{h-2}^2 \Lambda_{-23} \left(\frac{H_{hot}}{1 \text{ kpc}} \right)^2 \left(\frac{R_{hot}}{3 \text{ kpc}} \right)^2 \text{ erg s}^{-1} \quad (43c)$$

where the rates \dot{M}_{ev} , \dot{M}_* are in M_\odot /yr. Here \dot{E}_{in} is the thermal energy injected into the hot corona by evaporating

cold gas at a rate \dot{M}_{ev} , \dot{E}_{SNII} is the energy supplied to the corona by Type II supernovae forming above and below one scale height of the cold gas layer and the parameter ϵ_{SNII} expresses the efficiency with which this energy is coupled to the hot coronal gas. \dot{E}_{cool} is the rate of energy lost by a uniform density isothermal corona of scale height H_{hot} within a cylinder of radius R_{hot} . For a large galaxy such as the Milky Way that can sustain an evaporation rate of $\sim 10 M_\odot$ /yr, \dot{E}_{cool} is small compared to \dot{E}_{in} and it is a good approximation to neglect radiative cooling in the early stages of the flow (see Appendix B). However, in a dwarf galaxy \dot{E}_{cool} is typically larger than \dot{E}_{in} . In this case, we expect that the hot component will develop a sonic point at a characteristic cooling scale height H_{cool}

$$H_{cool} \sim v_w t_{cool} \sim 11 \left(\frac{v_w}{100 \text{ km/s}} \right) T_{h6} n_{h-2}^{-1} \Lambda_{-23}^{-1} \text{ kpc.} \quad (44)$$

(see *e.g.* Kahn 1981 and Appendix B) and that most of the thermal energy will be converted into kinetic energy by the time the gas flows to H_{cool} . We therefore ignore radiative cooling and estimate the bulk velocity of the wind at each radial shell in the disc from

$$\frac{1}{2} \dot{M}_{out}^\Omega v_w^2 = \dot{E}_{in}^\Omega + \dot{E}_{SNII}^\Omega, \quad (45a)$$

and to close the equations we assume that

$$\dot{M}_{out}^\Omega = \dot{M}_{in}^\Omega = \dot{M}_{ev}^\Omega. \quad (45b)$$

(Note that the numerical coefficient in equation (43a) has been adjusted to give $v_w = \sqrt{2.5}c_i$ if $\dot{E}_{SNII} = 0$ so that the criterion for the wind to escape, $v_w > v_{esc}$, is the same as in the preceding Section).

Energy input from Type II supernovae exploding high above the cold gas layer will make a small contribution to the thermal energy of the hot coronal gas. For values of $\epsilon_{SNII} \sim 1$, \dot{E}_{SNII}^Ω will be about 20% or so of \dot{E}_{in} and cannot be higher because \dot{M}_{ev}^Ω and the star formation rate are nearly proportional to each other (equation 27). Type Ia supernovae will also supply energy to the corona, with a time lag of perhaps $\gtrsim 1$ Gyr (Madau, Della Valle and Panagia 1998). However, this effect will also make a small perturbation to the energy budget of the corona and so it is ignored here. Furthermore, in the models described here much of the gas is expelled on a timescale of $\lesssim 1$ Gyr, thus feedback is likely to be more or less complete before energy injection from Type Ia supernovae becomes significant.

5.4 Pressure equilibrium and cold cloud radii

In the models of Section 3 and 4, the cold cloud radii were kept constant irrespective of the pressure of the confining hot phase. More realistically, the cold cloud radii will adjust to maintain approximate pressure equilibrium with the hot phase. Thus

$$\frac{a}{a_\odot} \approx 0.53 \left(\frac{T_c}{80K} \right)^{1/3} (n_{h-2} T_{h6})^{-1/3}, \quad (46)$$

where a_\odot denotes the cloud radii at the solar neighbourhood with values as given in equation (17) and T_c is the internal temperature of the cold clouds. In our own Galaxy, photoelectric heating of dust grains is believed to be the main heating mechanism of the cold clouds (see *e.g.* Wolfire *et al.*

1995) but other heating mechanisms may be important, for example, cosmic-ray heating (Field, Goldsmith and Habing 1969). We therefore expect that T_c varies in a complex (and uncomputable) way as a galaxy evolves. To assess the effects of the pressure response of the cold clouds, T_c will be assumed to remain constant at 80K. The cloud radii are then determined solely by the pressure of the hot component via equation (46).

The energy lost through cloud collisions (equation 18) varies as a^2 (for fixed cloud masses). However, the cloud heating efficiency factor ϵ_c will also change as the cloud radii change in response to the pressure of the hot phase. In the model of MO77, the energy acquired from momentum exchange with cooling supernovae shells varies as a^4 . The net effect of these variations in the self-regulating star formation model is to introduce positive feedback, since a higher rate of star formation is required to balance energy lost through cloud collisions in regions where the ambient pressure is higher. This is modelled by assuming $\dot{E}_{coll} \propto (a/a_\odot)^2$ and $\epsilon_c = \epsilon_{c\odot}(a/a_\odot)^4$, where $\epsilon_{c\odot}$ is a fiducial efficiency factor.

5.5 Induced star formation

The maximum mass for an isothermal cloud in pressure equilibrium with the confining medium of pressure p_h is given by the Bonner-Ebert criterion (Bonner 1956, Ebert 1955, Spitzer 1968),

$$\begin{aligned} m_{BE} &= 1.18 \left(\frac{kT_c}{\mu_p} \right)^2 G^{-3/2} p_h^{-1/2} \\ &= 433 \left(\frac{T_c}{80K} \right)^2 (n_h - 2T_{h6})^{-1/2} M_\odot. \end{aligned} \quad (47)$$

For our own Galaxy (MO77), $n_h \sim 1.5 \times 10^{-3} \text{cm}^{-3}$, $T_h \sim 4 \times 10^5$ and $p_h \sim 3 \times 10^{-12} \text{dyne cm}^{-2}$, hence $m_{BE} \approx 1700M_\odot$. This is reasonably close to the upper mass limit, $m_u = 4300M_\odot$, for the cold cloud mass spectrum adopted in this paper ($a_u = 10\text{pc}$ with $\rho_c = 7 \times 10^{-23} \text{g/cm}^3$). Gravitational stability requires $m_u \approx m_{BE}$ and we will henceforth impose this condition in determining the upper mass limit of the cold cloud spectrum. An increase in the pressure of the hot phase will lead to a decrease in m_u and hence to some pressure induced star formation. If the over-pressured clouds fragment into stars with an efficiency ϵ_{BE} , the induced star formation rate is given by

$$\frac{dM_s^\Omega}{dt} = \epsilon_{BE} \frac{M_g^\Omega}{2p_h \ln(m_u/m_L)} \begin{cases} dp_h/dt & dp_h/dt > 0 \\ 0 & dp_h/dt \leq 0 \end{cases}, \quad (48)$$

where m_L is the lower limit to the cloud mass spectrum, $m_L \approx 0.5M_\odot$. This provides an additional source of positive feedback, since as the pressure of the hot component rises the star formation rate of the self-regulating model is enhanced by pressure induced star formation.

5.6 Chemical evolution

It is straightforward to include chemical evolution in the models using the instantaneous recycling approximation. We distinguish between ‘primordial’ infalling gas accreting at a rate $d\mu_I/dt$ with metallicity Z_I , and processed gas from the

galactic fountain of metallicity Z_F accreted at a rate $d\mu_F/dt$. The equation of chemical evolution is then

$$\mu_g dZ = p d\mu_s + (Z_I - Z) d\mu_I + (Z_F - Z) d\mu_F, \quad (49)$$

(see *e.g.* Pagel 1997), where p is the yield. We adopt a yield of $p = 0.02$ and assume that the primordial gas has zero metallicity ($Z_I = 0$). Gas ejected in a galactic fountain is assumed to have the same metallicity as the ISM at the time that the gas was ejected. Within the disc, the ISM gas is assumed to be perfectly mixed at all times. We normalize the metallicities to the solar value, for which we adopt $Z_\odot = 0.02$.

6 RESULTS AND DISCUSSION

6.1 Variation of input parameters

In addition to the many simplifying assumptions introduced in previous sections, the model described here has 4 key parameters: (i) ϕ_κ , determining the efficiency of heat conduction (equation 20); (ii) $\epsilon_{c\odot}$, controlling the star formation rate (equation 19); (iii) ϵ_{SNII} , determining the efficiency with which energy from Type II supernovae couples directly to the gas (equation 45a); (iv) ϵ_{BE} , setting the efficiency with which over-pressured ISM clouds collapse to make stars (equation 48). In addition, the ISM cloud radii can be allowed to vary in response to the pressure of the ISM as described in Section 5.4.

The effects of varying these parameters are summarised in Table 2. Here we have run six models of galaxies MW and DW varying the input parameters. We list the final stellar mass M_s , gaseous disc mass M_g , and ejected mass M_{ej} after 10 Gyr for model DW (there is very little evolution after this time) and after 15 Gyr for model MW. The parameters f_{ej} and f_* are the final ejected and stellar masses divided by the total baryonic mass ($M_{ej} + M_* + M_g$). τ_{ej} is the time when half the final ejected mass is lost. The last three numbers list the final mean metallicities of the cold ISM, the stars and the ejected gas.

The most important result from this table is that the final parameters of the models are remarkably insensitive to variations of the input parameters. For models DW, the final stellar disc mass varies between $\sim 4 \times 10^7$ and $7 \times 10^7 M_\odot$ and the gas ejection fraction varies from 0.59 to 0.82. For models MW, the final stellar disc mass varies between $\sim 2.3 \times 10^{10}$ and $2.8 \times 10^{10} M_\odot$ and the gas ejection fraction varies from 0.12 to 0.22. Figure 10 shows the evolution of the radial density profiles of models MW1 and DW1 and figure 11 shows the time evolution of the star formation rates, gas fractions and gas velocity dispersions. The models of Table 2 behave in similar ways, and so these two figures are representative of the behaviour of all of the models. These figures are qualitatively similar to those of the simple model of Section 4 (figure 8 and 9). The main differences are:

- (a) The gas discs have a sharper outer edge. This is a consequence of the infall model; the outer edge is determined by the final time of the model which sets the maximum cooling radius within the halo (*cf.* figures 7).
- (b) The radial profiles of models MW show oscillatory behaviour near their centres, and the star formation rates and gas fractions show oscillatory behaviour as a function of

Table 2: Feedback Efficiency: Variation of Input Parameters

Model	MW1	DW1	MW2	DW2	MW3	DW3
ϕ_κ		0.1		0.01		0.1
$\epsilon_{c\odot}$		0.01		0.01		0.03
ϵ_{SNII}		0.0		0.0		1.0
ϵ_{BE}		0.0		0.0		0.0
§5.4		no		no		no
$M_s (M_\odot)$	2.8×10^{10}	4.2×10^7	2.3×10^{10}	7.1×10^7	2.3×10^{10}	3.6×10^7
$M_g (M_\odot)$	5.4×10^9	1.3×10^8	5.4×10^9	9.9×10^7	6.9×10^9	1.3×10^8
$M_{ej} (M_\odot)$	4.6×10^9	2.6×10^8	7.9×10^9	3.1×10^8	6.5×10^9	3.0×10^8
f_{ej}	0.12	0.59	0.22	0.64	0.18	0.64
τ_{ej} (Gyr)	0.25	0.82	0.40	1.8	0.30	1.24
f_*	0.74	0.10	0.63	0.15	0.63	0.08
$\langle Z_g/Z_\odot \rangle$	0.65	0.03	0.57	0.04	0.56	0.02
$\langle Z_s/Z_\odot \rangle$	0.55	0.20	0.43	0.30	0.42	0.19
$\langle Z_{ej}/Z_\odot \rangle$	0.29	0.11	0.38	0.14	0.26	0.09

Model	MW4	DW4	MW5	DW5	MW6	DW6
ϕ_κ		0.1		0.1		0.1
$\epsilon_{c\odot}$		0.01		0.01		0.01
ϵ_{SNII}		1.0		1.0		1.0
ϵ_{BE}		0.0		0.05		0.05
§5.4		yes		no		yes
$M_s (M_\odot)$	2.5×10^{10}	4.3×10^7	2.4×10^{10}	4.3×10^7	2.5×10^{10}	4.5×10^7
$M_g (M_\odot)$	2.1×10^9	3.5×10^7	4.9×10^9	9.5×10^7	1.9×10^9	2.9×10^7
$M_{ej} (M_\odot)$	7.1×10^9	3.4×10^8	6.8×10^9	3.1×10^8	7.2×10^9	3.4×10^8
f_{ej}	0.21	0.82	0.19	0.69	0.21	0.82
τ_{ej} (Gyr)	0.30	1.19	0.30	1.19	0.21	1.12
f_*	0.73	0.10	0.67	0.09	0.74	0.11
$\langle Z_g/Z_\odot \rangle$	0.62	0.03	0.59	0.02	0.64	0.02
$\langle Z_s/Z_\odot \rangle$	0.47	0.17	0.44	0.21	0.48	0.19
$\langle Z_{ej}/Z_\odot \rangle$	0.26	0.09	0.27	0.10	0.27	0.10

time. Both of these effects are a consequence of the galactic fountain.

In these models, the star formation rate begins to rise as the gas disc builds up from infalling gas. As the star formation rate rises, the cold ISM is converted efficiently into a hot phase and this is either driven out of the halo or becomes part of the galactic fountain. In models MW, most of the gas that escapes from the system is lost within this early ($\lesssim 0.2$ Gyr) period of star formation when the net star formation rate is close to its peak of $\sim 10M_\odot/\text{yr}$. After about 0.2 Gyr, the temperature of the hot phase in models MW settles to $\sim 10^6$ K very nearly independent of radius (*cf* figure 10), and so the galactic fountain cycles on a characteristic time-scale of $\sim 4 \times 10^8$ yr. Models DW behave in much the same way as the simpler models of Section 4.3, except that infall, by construction, extends over a longer period of time. In these models, the escape criterion for the wind is satisfied over most of the lifetime of the disc and hence the model of a galactic fountain is unimportant.

We discuss briefly the effects of varying the input parameters:

ϕ_κ : The evaporation rate \dot{M}_{ev} has a weak dependence on the evaporation parameter ϕ_κ ($\propto \phi_\kappa^{0.29}$, equation 28) and obviously decreases as ϕ_κ is reduced. However, the temperature of the hot component is proportional to $\phi_\kappa^{-0.29}$ and hence rises as ϕ_κ is reduced. The net effect is that the mass of gas

ejected is relatively insensitive to ϕ_κ , but the mass of the final stellar disc increases as ϕ_κ is reduced.

$\epsilon_{c\odot}$: Increasing this parameter reduces the star formation rate in the self-regulating model for a fixed gas surface density and velocity dispersion (equations 15 and 18). However, a lower past star formation rate leads to a higher gas surface density which increases the star formation rate. These effects tend to cancel and so the models are insensitive to variations in $\epsilon_{c\odot}$.

ϵ_{SNII} : Setting this parameter to unity increases the temperature of the hot component slightly and hence increases the efficiency of feedback. As explained in Section 5.3, energy injection by Type II supernovae at large vertical scale heights will always be small compared to the internal energy of the hot phase.

ϵ_{BE} : Values of $\epsilon_{\text{BE}} \sim 0.05$ have little effect on the evolution. Provided that ϵ_{BE} is not too large (so that it does not dominate the net star formation rate), pressure enhanced star formation is self-limiting because it increases the velocity dispersion of the cold clouds (reducing the star formation rate in the self-regulating model) and converts cold gas to hot gas. Both of these effects tend to reduce the net star formation rate.

Pressure response of cold cloud radii: Allowing the cold gas radii to respond to the pressure of the hot phase provides

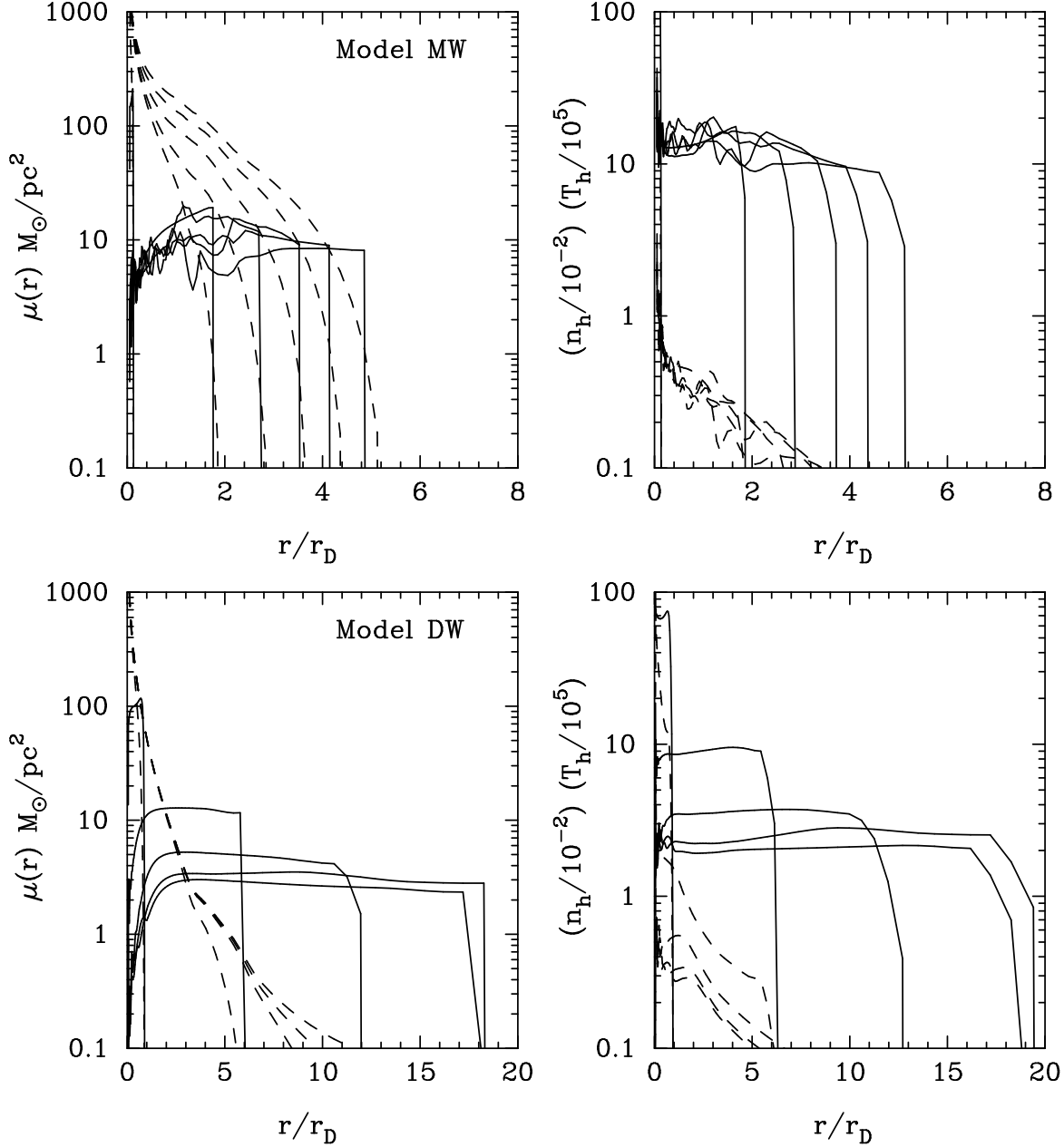


Figure 10. The left hand panels show the evolution of the stellar (dashed lines) and cold gas (solid lines) profiles in models MW1 and DW1. The right hand panels show the temperature (solid lines) and density (dashed lines) of the hot component. The radius r_D is the fiducial radius listed in Table 1. The results are plotted at ages of 0.1, 1, 3, 6, 10 Gyr and (for MW1 only) at 15 Gyr.

strong positive feedback in the very early stages of galaxy formation when the pressure of the hot phase is high. However, most of the cold ISM is ejected on a much longer timescale (*cf.* values of τ_{ej} in Table 2) when the typical pressure of the ISM is similar to that in our own Galaxy. The pressure response of the cold cloud radii therefore has little effect on the final feedback efficiency.

The models described here involve a complex set of coupled equations and a number of parameters. However, one of the most interesting aspects of this study is that the equations interact in such a way that the evolution of the models is insensitive to the parameters. Most importantly, the efficiency of feedback is insensitive to the thermal conduction

parameter ϕ_κ . The possible severe suppression of thermal conduction by tangled magnetic fields in astrophysical environments is a long standing theoretical problem. However, our results show that even a reduction of κ by a factor of 100 or more will not significantly alter the efficiency of feedback.

6.2 Chemical evolution

In this section, we summarize some of the results relating to chemical evolution in these models. Our intention is not to present a detailed model of chemical evolution in disc systems along the lines of, for example, Lacey and Fall (1983, 1985) but to investigate some of the general features of chem-

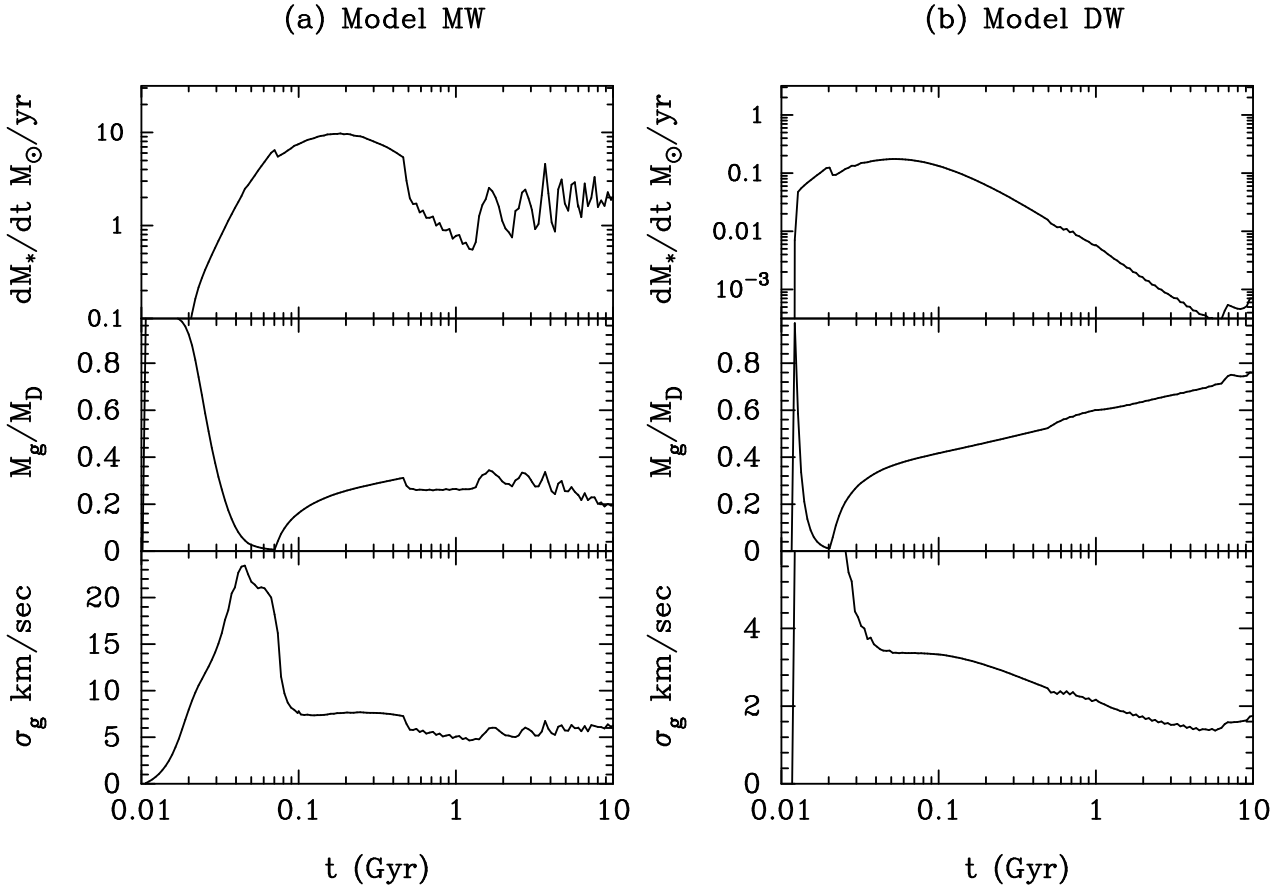


Figure 11. Evolution of the star formation rate, gas fraction and gas cloud velocity dispersion for the models shown in figure 10.

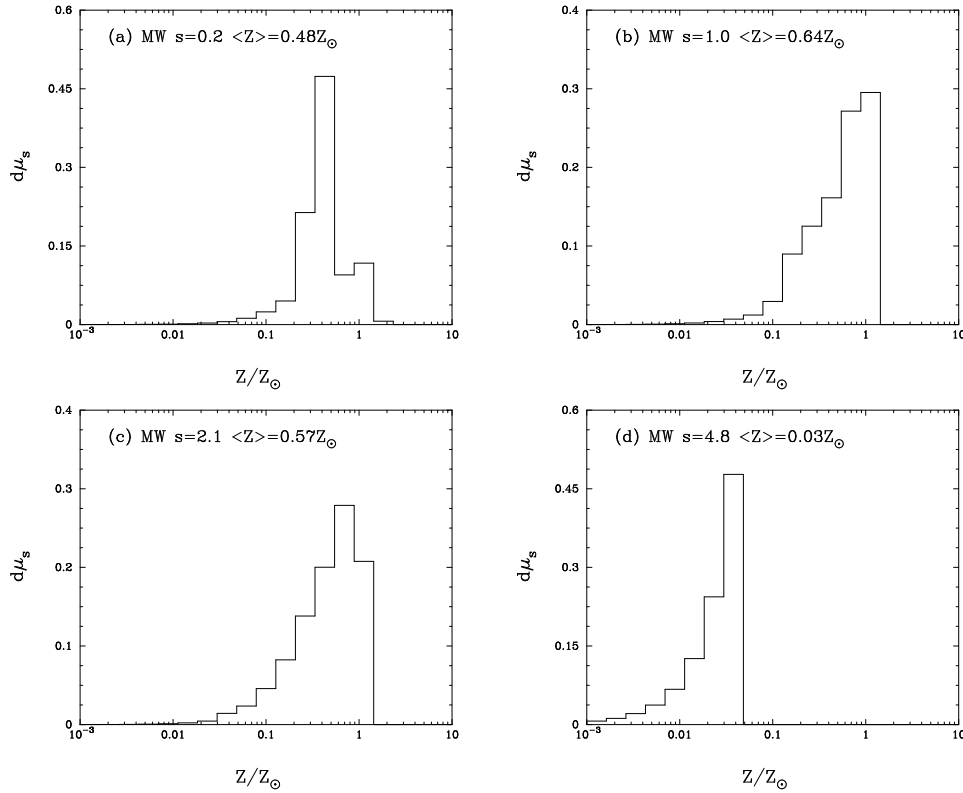


Figure 12. The distribution of stellar metallicities at four radii in model MW1 at an age of 15 Gyr.

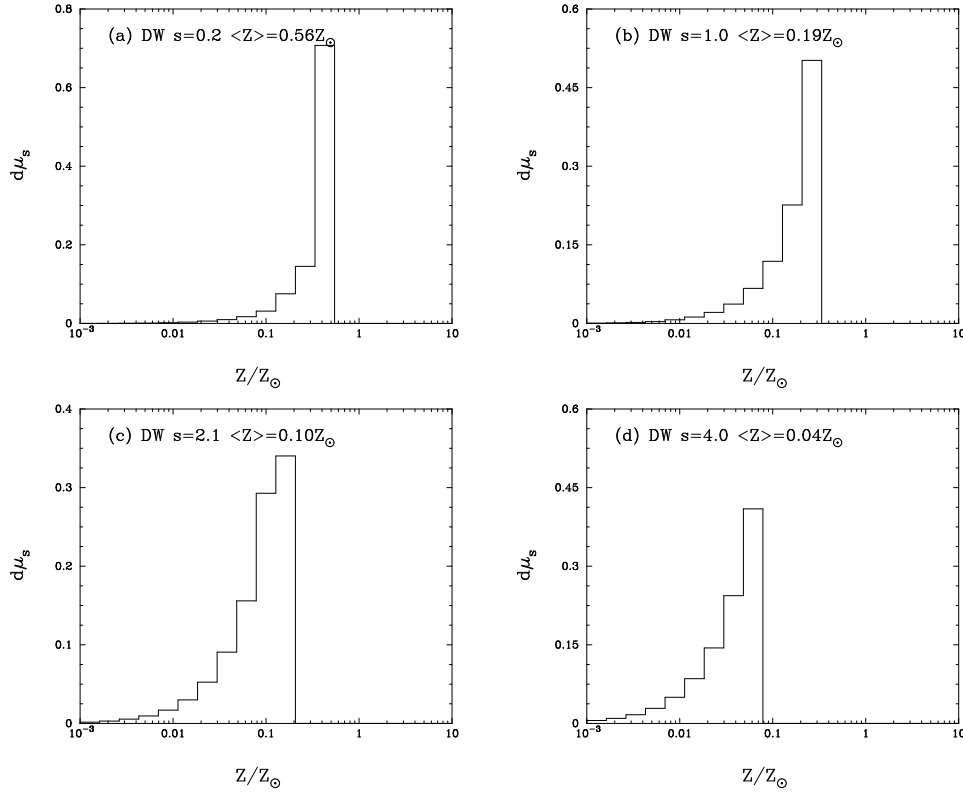


Figure 13. The distribution of stellar metallicities at four radii in model DW1 at an age of 10 Gyr.

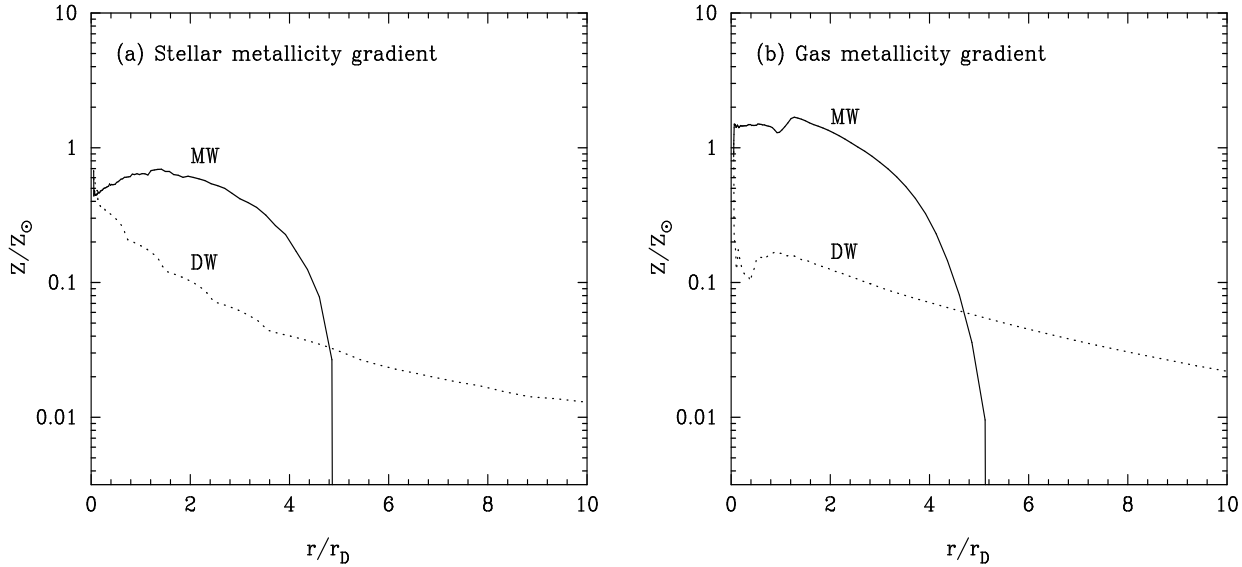


Figure 14. Metallicity gradients in the stars and gas at the final times in models MW1 and DW1

ical evolution with physically motivated models of inflow and outflow. The chemical evolution model is based on the instantaneous recycling approximation as described in Section 5.6. This is probably a reasonable approximation since the timescales of star formation and outflow are ~ 1 Gyr, but will overestimate the gas metallicities where the gas density is low. As in the previous Section, results from models MW1 and DW1 are used to illustrate the general features of the models. The other models listed in Table 2 behave in very similar ways.

6.2.1 Stellar metallicity distribution

The final mean stellar metallicities are typically $Z_s/Z_\odot \approx 0.5$ in models MW and ≈ 0.2 in models DW. Models DW have a lower stellar metallicity because a larger fraction of the ISM is expelled in a wind. The stellar metallicity distributions are shown in Figures (12) and (13). Figure (12c) is particularly interesting because this radius is close to the solar radius. This metallicity distribution is quite similar to that of G-dwarfs in the solar cylinder (see *e.g.* figure 8.19

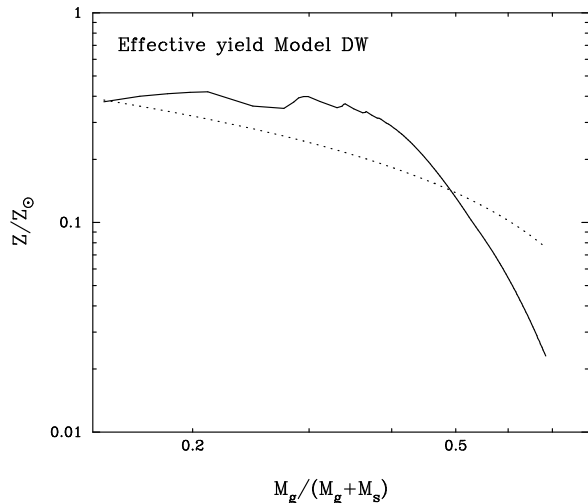


Figure 15. The effective yield for model DW1. For each radial ring in the galaxy we plot the gas metallicity Z_g against the gas fraction in that ring. According to the simple closed box model of chemical evolution, $Z_g = -p \ln(M_g/(M_g + M_s))$, where p is the yield. The dashed line shows this relation, but using an effective yield $p_{\text{eff}} = p/5$.

of Pagel 1997), showing that the infall model solves the ‘G-dwarf’ problem of closed box models of chemical evolution. The metallicity distributions of model DW1 plotted in figure (13) also show a lack of stars with low metallicities.

6.2.2 Metallicity gradients

Over most of the stellar disc, model MW1 has a fairly weak stellar metallicity gradient (figure 14a) except at the very outer edge where the stellar density and metallicity fall abruptly. This differs from the metallicity gradients seen in large disc systems which show linear gradients (see Vila-Costas 1998 for a recent review). It is possible that this problem might be resolved by including radial gas flows in the models (Lacey and Fall 1985, Pitts and Tayler 1985). The stellar metallicity gradients in model DW1 are steeper, in qualitative with observations which indicate that the abundance gradients in Scd and Irr galaxies are steeper than those in earlier type galaxies.

The radial gas metallicity profiles are shown in figure (14b). Model DW contains a gaseous disc extending well beyond the edge of the stellar disc. This gas disc has a low metallicity in the outer parts, with $Z/Z_{\odot} \lesssim 10^{-2}$ at $r \gtrsim 2$ kpc. At these large radii, the star formation rate is always low and the gas disc can survive for much longer than a Hubble time without converting into stars. This is unlikely to happen in all galaxies for at least two reasons: (i) the energy injection from supernovae into this gas will not be uniform as assumed in this paper; (ii) the extended gas disc is susceptible to external disturbances and so could be tidally stripped or transported towards the centre of the system in a tidal interaction. Nevertheless, it is possible that dwarf galaxies at high redshift possess extended gaseous discs, some of which survive to the present day.

6.2.3 Effective yields

According to the simple closed box model of chemical evolution, the metallicity of the ISM is related to the gas fraction according to

$$Z_g = -p \ln(M_g/(M_g + M_s)). \quad (50)$$

It is well known that the yields derived from applying this relation to gas rich galaxies (usually dwarf systems) result in ‘effective yields’, p_{eff} , that are much lower than the yield expected from a standard Salpeter-like IMF. For example, Vila-Costas and Edmunds (1992) find effective yields in the range $p_{\text{eff}} \sim 0.004$ – 0.02 and that the effective yield decreases with increasing radius.

The solid line in figure (15) shows the final gas metallicity in radial rings in model DW1 plotted against the gas fraction within each ring. The dashed line shows equation (50) with an effective yield of 0.004 (*i.e.* one-fifth of the true yield). The strong outflows in this model suppress the effective yield well below the true yield and produce a strong radial variation of the effective yield, in qualitative agreement with observations.

6.2.4 Metallicity of ejected gas

The last line in Table 2 lists the mean metallicity of the gas that escapes from the galaxy. The mean metallicity of the ejected gas is about $0.3Z_{\odot}$ for model MW1 and about $0.1Z_{\odot}$ for model DW1. In model DW1 this value is about 3 to 5 times higher than the mean metallicity of the final gas disc. The ejected gas in this model is therefore ‘metal enhanced’ relative to the gaseous disc. The mechanism for this metal enhancement is physically different to that in the models of Vader (1986, 1987) and Mac Low and Ferrara (1999). In the models of these authors, metal enhancement arises from incomplete local mixing between the supernovae ejecta and the ISM. In our models, the gas is assumed to be well mixed locally, but metal enhancement arises because the gas is lost preferentially from the central part of the galaxy, which has a higher metallicity than the gas in the outer parts of the system.

6.3 Connection with damped Lyman alpha systems

The column density threshold for the identification of damped Ly α systems is $N(\text{HI}) \gtrsim 2 \times 10^{20} \text{ cm}^{-2}$ (Wolfe 1995) corresponding to a neutral gas surface mass density of $\sim 1.6 M_{\odot}/\text{pc}^2$. Comparison with Figure 10 shows that the extended cold gaseous discs around dwarf galaxies would be detectable as damped Ly α systems. Furthermore, in CDM-like models, such extended discs around dwarf galaxies would dominate the cross-section for the identification of damped Ly α systems at high redshift because the space density of haloes with low circular speeds is high (Kauffman and Charlot 1994, Mo and Miralda-Escude 1994). If this is the case, then the metallicities of damped Ly α systems would be expected to be low at high redshift, $Z/Z_{\odot} \sim \text{few} \times 10^{-2}$, with occasional lines-of-sight intersecting the central regions of galaxies where the metallicity rises to $Z/Z_{\odot} \gtrsim 0.1$. At lower redshifts, the metallicities of damped systems would be expected to show a similarly large scatter, but with perhaps

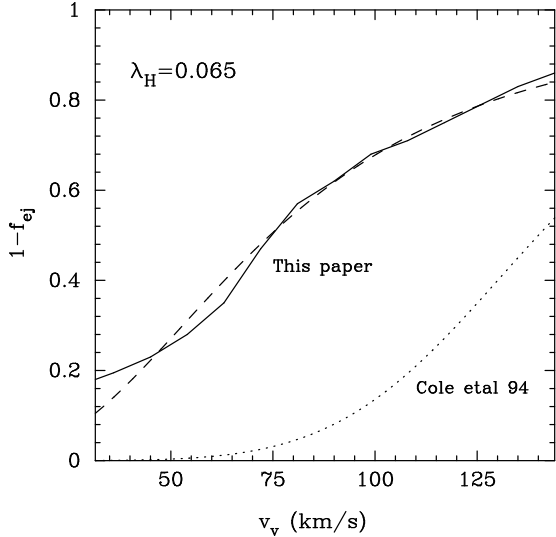


Figure 16. The solid line shows the retained baryonic fraction $1 - f_{ej}$ as a function of the halo circular speed v_v . The parameters ϕ_κ , $\epsilon_{c\odot}$ etc. adopted are the same as those of models MW4 and DW4 listed in Table 2. The dotted line shows the relation adopted by Cole *et al.* (1994), equation (51) with $v_{hot} = 140 \text{ km s}^{-1}$ and $\alpha_{hot} = 5.5$. The dashed line shows equation (51) with $v_{hot} = 75 \text{ km s}^{-1}$ and $\alpha_{hot} = 2.5$.

a trend for the mean metallicity to increase as disc systems with higher circular speeds form and the extended gaseous discs around dwarfs are disrupted by tidal encounters.

This is qualitatively in accord with what is observed (Pettini *et al.* 1997, Pettini *et al.* 1999, Pettini 1999). These authors find that the typical metallicity of a damped Ly α system at $z \sim 2-3$ is about $0.08Z_\odot$ with a spread of about two orders of magnitude. Comparing the metallicities of high redshift systems with those of 10 damped Ly α systems with redshifts $z = 0.4-1.5$, Pettini *et al.* (1999) find no evidence for evolution of the column density weighted metallicity. Whether these and other properties of the damped Ly α systems can be reproduced with the feedback model described here requires more detailed ‘semi-analytic’ calculations along the lines described by Kauffmann (1996). However, the key point that we wish to emphasise is that according to the models described here, most of the cross-section at any given redshift will be dominated by largely unprocessed gas in the outer parts of galaxies that does not participate in the star formation process. The metallicity distributions and the evolution of Ω_{HI} as a function of redshift are therefore more likely to tell us about feedback processes and the outer parts of dwarf galaxies than about the history of star formation. Attempts to use the properties of damped Ly α systems to constrain the cosmic star formation history (*e.g.* Pei, Fall and Hauser 1999) should therefore be viewed with caution.

6.4 Feedback efficiency as a function of halo circular speed and semi-analytic models of galaxy formation

In this section we investigate the efficiency of feedback as a function of halo circular speed. We have adopted the param-

eters of models 4 in Table 1 and run a series of models varying the halo circular speed v_v . The virial radius of the halo is set to $r_v = 150(v_v/126 \text{ km s}^{-1})^2 \text{ kpc}$, the concentration parameter $c = 10$ and the ratio of gas to halo mass within the virial radius is set to $1/10$. The halo rotation speed is set by equation (39) with the fiducial disc scale length equal to $r_v/50$. With these parameters, the family of models has a constant value for the halo spin parameter of $\lambda_H = 0.065$.

The retained baryonic fraction, $1 - f_{ej}$, is plotted as a function of halo circular speed in Figure 16. The dotted line shows the relation used by Cole *et al.* (1994, hereafter C94) in their semi-analytic models,

$$1 - f_{hot} = \frac{1}{1 + \beta(v_v)}, \quad \beta(v_v) = \left(\frac{v_v}{v_{hot}}\right)^{-\alpha_{hot}}, \quad (51)$$

where f_{hot} is the fraction of the cooled gas that is reheated and v_{hot} and α_{hot} are parameters. C94 adopt a severe feedback prescription with $\alpha_{hot} = 5.5$ and $v_{hot} = 140 \text{ km s}^{-1}$ to reproduce the flat faint end slope of the B-band galaxy luminosity function in a critical density CDM model. The C94 feedback model does not agree at all well with the models described here. There is a slight ambiguity in the appropriate value of v_v to use in equation (51) because C94 adopt an isothermal rather than an NFW halo profile; the halo circular speed at $\sim 0.1r_v$ may be 20% higher than the circular speed at the virial radius, but this is far too small a difference to reconcile the C94 feedback prescription with the models of this paper.

In fact, the dashed line in Figure 16 shows that our models are reasonably well described by equation (51) with $v_{hot} = 75 \text{ km s}^{-1}$ and $\alpha_{hot} = 2.5$. Our results therefore suggest a much gentler feedback prescription than assumed in C94. Note that with the C94 parameters, a Milky Way type galaxy with $v_v \approx 130 \text{ km s}^{-1}$ would have lost about 60% of its baryonic mass in a wind. This is well outside the range found from our models for plausible choices of the input parameters (*cf.* Table 2).

Recently Baugh *et al.* (1999) and Cole *et al.* (1999) describe semi-analytic models applied to Λ -dominated CDM cosmologies that employ a gentler feedback model. The prescription for their reference model is similar to that of equation (51) with $v_{hot} = 150 \text{ km s}^{-1}$ and $\alpha_{hot} = 2.0$, but with v_v replaced by the disc circular speed v_{disc} . This model is closer to the results found here. Assuming angular momentum conservation, a halo with $\lambda_H \approx 0.06$ will produce a disc with a circular speed $v_{disc} \approx 1.7v_v$ (*cf.* Table 1) and so their model can be approximated by equation (51) with $v_{hot} \approx 90 \text{ km s}^{-1}$ and $\alpha_{hot} = 2.0$. With these parameters, their model gives somewhat stronger feedback than found in our models, but is well within the range of physical uncertainties. Kauffmann *et al.* (1993) and Kauffmann, Guiderdoni and White (1994) also adopt a much less severe feedback prescription than C94 in their semi-analytic models. For a detailed analysis of the effects of varying the feedback prescription (and other parameters) in semi-analytic models see Somerville and Primack (1999).

The change from an Einstein-de Sitter CDM cosmology in C94 to a Λ -dominated CDM model in Cole *et al.* (1999) partly explains why the revised models provide a reasonable match to observations using less efficient feedback. However, the revised models predict a faint end slope for the B-band luminosity function that is consistent with the observations

of Zucca *et al.* (1997) but not with those of other authors (*e.g.* Loveday *et al.* 1992, Maddox *et al.* 1998). (The earlier paper of Cole *et al.* 1994 attempted to reproduce the flat faint end slope of the Loveday *et al.* luminosity function). The observational differences in estimates of the faint end slope of the optical luminosity function are not properly understood and so it remains unclear whether a gentle feedback model, of the type proposed here and used in Cole *et al.* (1999), can account for galaxy formation in CDM-type models.

Table 3: Dependence of Feedback Efficiency of Model DW on Halo Angular Momentum

f_{coll}	v_c (km/s)	λ_H	f_{ej}
25	50	0.12	0.64
50	70	0.065	0.59
150	120	0.031	0.82

With the Cole *et al.* (1999) parameterization the efficiency of feedback depends, by construction, on the surface density of the galaxy and hence on the angular momentum of the parent halo. In their model, higher angular momentum haloes lead to more efficient feedback because they form low surface density discs with low disc circular speeds. This is not what is found in our models. Table 3 lists the ejected gas fraction as a function of the halo spin parameter λ_H . Here, the halo circular speed and virial radius, v_v and r_v , are the same as for model DW in Table 1, but the amplitude of the halo rotation speed (or equivalently the parameter f_{coll}) is adjusted to change the spin parameter of the halo. The parameters of the feedback model are the same as those for model DW1 in Table 2. The feedback efficiency depends weakly (and non-monotonically) on λ_H , and is greater in systems with low values of λ_H . This is because higher surface densities in low λ galaxies result in higher star formation rates and a higher temperature hot component that can escape more easily from the halo.

The timescale for feedback in C94 and Cole *et al.* 1999 is closely linked to the star formation timescale which is assumed to be shorter in galaxies with high circular speeds. This is not what is found in the models of Table 2. The timescale for star formation is of order several Gyr in models MW (which have a roughly constant star formation rate at late times, see Figure 11), yet the ejection of hot gas occurs only in the initial stages of formation with a characteristic timescale of ~ 0.3 Gyr. In models DW, the situation is reversed with star formation occurring on a somewhat shorter timescale than that for outflow.

7 CONCLUSIONS

The main aim of this paper has been to show that supernovae driven feedback can operate in a quiescent mode and that high rates of star formation are not required to drive efficient feedback. In dwarf galaxies feedback occurs on an infalling timescale and so can extend over a period of ~ 1 Gyr. In the feedback model developed here, cold gas clouds are steadily evaporated in expanding supernovae remnants and converted into a hot component. Critically, the rate at

which cold gas is evaporated can exceed the rate at which mass is converted into stars. If the temperature of the hot component is high enough, a wind will form and the hot gas can escape from the halo (provided the interaction with infalling gas can be ignored). If the temperature of the hot component is not high enough for it to escape from the halo, it will cool and fall back down to the disc in a galactic fountain. Some characteristic features of the models are as follows:

(i) In a Milky Way type system, feedback from supernovae may drive out some of the gas from the halo in the early phases of evolution ($t \lesssim 0.3$ Gyr) when the star formation rate is high and the temperature of the hot phase exceeds $\sim 5 \times 10^6$ K. For plausible sets of parameters, perhaps 20 – 30% of the final stellar mass might escape from the galaxy. At later times, the temperature of the hot phase drops to $T \sim 10^6$ K and the evaporated gas cycles within the halo in a galactic fountain.

(ii) In a dwarf galaxy with a circular speed ~ 50 kms $^{-1}$, expanding supernovae remnants can convert the cold interstellar medium efficiently into a hot component with a characteristic temperature of a few times 10^5 K. This evaporated gas can escape from the halo in a cool wind. Typically, only about 10% of the baryonic material forms stars. Gas accreted from the halo at $\gtrsim 1$ Gyr forms an extended gaseous disc which, according to the self-regulating star formation model used here, can survive for longer than a Hubble time without converting into stars.

(iii) The feedback model developed here is meant to provide a sketch of how feedback might operate in a multi-phase interstellar medium. The model contains a number of obvious over-simplifications. For example, we have neglected any interaction of the outflowing gas with the infalling medium, we have not addressed the origin of the cold cloud spectrum, ignored the dense molecular cloud component of the ISM and neglected any local dissipation of supernovae energy in star forming regions. These effects, and other processes, are undoubtedly important in determining the efficiency of feedback. Nevertheless, the simplified model presented here contains some interesting features. Firstly, the model shows how positive feedback (via pressure induced star formation) and negative feedback (via outflowing gas) can occur *simultaneously*. Secondly, the models are remarkably insensitive to uncertain physical parameters, in particular, thermal conduction would need to be suppressed relative to its ideal value by factors of much more than 100 to qualitatively change the model. If thermal conduction is highly suppressed, it may be possible to construct a qualitatively similar model to the one presented here in which cold gas is converted into hot gas in shocks.

(iv) The self-regulated star formation and feedback models described here provide physically based models for the star formation timescale and feedback efficiency as a function of the parameters of the halo. The star formation timescale and feedback efficiency (or timescale) are taken as free parameters in semi-analytic models of galaxy formation (*e.g.* Cole *et al.* 1999, Kauffmann *et al.* 1994) and are critically important in determining some of the key predicted properties of these models, for example, the faint end slope of the galaxy luminosity function and the star formation history at high redshifts (see *e.g.* Somerville and Primack 1999). It

is therefore important that we develop a theoretical understanding of these parameters (as attempted crudely here) and also that ways are found to constrain these parameters observationally. The results presented here show that supernovae feedback is much less effective than assumed in some earlier semi-analytic models (Cole *et al.* 1994, Baugh *et al.* 1996) but is closer to the more gentler feedback prescriptions used in more recent models (Cole *et al.* 1999, Somerville and Primack 1999).

The feedback model described in this paper has a number of consequences and raises some problems which are summarized below.

(i) *Evidence for outflows:* According to the models described here, outflows with speeds of $\sim 200 T_{h6}^{1/2} \text{ kms}^{-1}$ should be common in high redshift galaxies. There is evidence for an outflow of $\sim 200 \text{ kms}^{-1}$, a mass loss rate of $\sim 60 M_{\odot}/\text{yr}$ and a star formation rate of $\sim 40 M_{\odot}/\text{yr}$ in the gravitationally lensed Lyman break galaxy MS1512-cB58 (Pettini *et al.* 2000). The outflow velocity in this galaxy is consistent with our models, but the star formation and mass loss rates (which are highly uncertain) are high. The most likely explanations are either that MS1512-cB58 is a massive galaxy driving an outflow that will remain bound to the system, or that it is a less massive system undergoing a burst of star formation. In addition to direct detection of outflowing gas, winds may have other observational consequences. The winds from dwarf galaxies will cool rapidly (see Appendix B). Wang (1995b) has suggested that photoionized gas clouds formed in the cooling wind might contribute to the Ly α forest. Nulsen, Barcon and Fabian (1998) suggest that outflows caused by bursts of star formation in dwarf galaxies might even produce damped Ly α systems.

(ii) *Damped Ly α systems:* The extended gaseous discs that form around dwarf galaxies in our models have low metallicities because they have low rates of star formation. If this is correct, then this largely unprocessed gas would dominate the cross section for the formation of damped Ly α absorbers. The metallicities of most of these systems would be low, but would show a large scatter because some lines of sight will pass close to the central regions of galaxies containing gas of high metallicity. This is broadly in agreement with what is observed. Extended gaseous discs would be vulnerable in tidal interactions. Some of the gas might be stripped and some might be transported into the central regions to be converted into stars and hot gas. The evolution of Ω_{HI} determined from damped Ly α systems (*e.g.* Storrie-Lombardi, McMahon and Irwin 1996) might have more to do with infall, feedback and tidal disruption than with the cosmic star formation history.

(iii) *Angular momentum conservation:* In hydrodynamic simulations, gas is found to cool effectively in sub-units during the formation of a protogalaxy. These sub-units lose their orbital angular momentum to the halo as they spiral towards the centre and merge. Hence the gas does not conserve angular momentum during the formation of a massive galaxy. (Navarro and Benz 1991, Navarro and Steinmetz 1997, Weil Eke and Efstathiou 1998, Navarro and Steinmetz 2000). In fact, in the absence of feedback it has proved impossible to form discs with angular momenta similar to those of real disc galaxies starting from CDM initial conditions. In the models described here, it has been assumed for simplicity that the

specific angular momentum of the gas is conserved during collapse. This assumption could easily be relaxed. However, the feedback model described here suggests that the numerical simulations miss some important physics. Firstly, it is preferentially the low angular momentum gas, infalling in the early stages of evolution, that is most likely to be ejected from a developing protogalaxy. Secondly, supernovae driven feedback may help to solve the angular momentum momentum problem by ejecting gas efficiently from sub-units. The ejected gas may then infall at later times when the halo is less sub-structured, approximately conserving its angular momentum (Weil *et al.* 1998, Eke, Efstathiou and Wright 2000).

(iv) *Implementing feedback in numerical simulations:* There have been a number of attempts to implement supernovae feedback in gas dynamical numerical simulations (*e.g.* Katz 1992, Navarro and White 1993, Navarro and Steinmetz 2000). These involve either heating the gas around star forming regions (which is ineffective because the energy is quickly radiated away) or reversing the flow of infalling gas. An implementation of the feedback model described here is well beyond the capabilities of present numerical codes. It would require modelling several gas phases, a cold interstellar medium, a hot outflowing medium and an infalling component, including mass transfer between each phase. It might be worth attempting simpler simulations in which cold high density gas is added to the halo beyond the virial radius at a rate that is determined by the local star formation rate.

(vi) *Starbursts vs quiescent feedback:* It is likely that starbursts are more common at high redshift because of the increased frequency of galaxy interactions. Starbursts could contribute to supernovae driven feedback in addition to the quiescent mode described here. However, at any one time, our models suggest that the cold gas component will have a mass of only 20 – 50% of the the mass of the stellar disk. Even if a substantial fraction of this gas is transported towards the centre of a galaxy in a tidal encounter (see *e.g.* Barnes and Hernquist 1996) and is subsequently ejected in a superwind, this mode of feedback will be inefficient because the mass of gas involved is a small fraction of the total gas mass ejected in the quiescent feedback mode over the lifetime of the galaxy.

(vii) *Metallicity ejection:* The mean metallicity of the gas ejected from a dwarf galaxy is typically about $Z_{\odot}/10$ in our models, and comparable to the mean metallicity of the stars in the final galaxy. Yet typically a dwarf galaxy is predicted to expel 5 to 10 times its residual mass in stars. Dwarf galaxies can therefore pollute the IGM with metals to a much higher level than might be inferred from their stellar content. The high metallicity of gas in the central regions of clusters $\sim Z_{\odot}/3$ (*e.g.* Mushotsky and Loewenstein 1997) may require a top-heavy IMF and gas ejection from massive galaxies.

Acknowledgments: The author acknowledges the award of a PPARC Senior Fellowship.

REFERENCES

- Babul A., Rees M.J., 1992, MNRAS, 255, 346.
- Barnes J., Efstathiou G., 1987, ApJ, 319, 575.
- Barnes J., Hernquist L., 1996, ApJ, 471, 115.
- Baugh C.M., Cole S., Frenk C.S., 1996, MNRAS, 283, 1361.
- Baugh C.M., Cole S., Frenk C.S., Lacey C.G., 1998, ApJ, 498, 504.
- Baugh C.M., Benson A.J., Cole S., Frenk C.S., Lacey C.G., 1999, astro-ph/9907056.
- Binney J., Tremaine S., 1987, *Galactic Dynamics* Princeton University Press, Princeton.
- Bonner W.B., 1956, MNRAS, 116, 351.
- Bregman J.N., 1980, ApJ, 236, 577.
- Bryan G.L., Machacek, M., Anninos P., Norman M.L., 1999, ApJ, 517, 13.
- Burke J.A., 1968, MNRAS, 140, 241.
- Burton W.B., 1991, in *The Galactic Interstellar Medium*, Saas-Fé Advanced Course 21, Springer-Verlag, Berlin.
- Cen R., Miralda-Escude J., Ostriker J.P., Rauch M., 1994, ApJ, 437, L9.
- Cole S., Aragon-Salamanca A., Frenk C.S., Navarro J.F., Zepf S., 1994, MNRAS, 271, 781.
- Cole S., Lacey C.G., Baugh C.M., Frenk C.S., 1999, MNRAS, submitted.
- Dekel A., Silk J., 1986, ApJ, 303, 39.
- Ebert R., 1955, Zs. f. Ap., 37, 217.
- Efstathiou G., 1992, MNRAS, 265, 43p.
- Efstathiou G., Ellis R.S., Peterson B.A., 1988, MNRAS, 232, 431.
- Eke V., Efstathiou G., Wright L., 2000, MNRAS, submitted.
- Ellis R.S., 1997, ARAA, 35, 389.
- Fabian A., 1999, MNRAS, 308, L39.
- Fall S.M., Efstathiou G., 1980, MNRAS, 193, 189.
- Fall S.M., Rees M.J., 1985, ApJ, 298, 18.
- Freeman K.C., 1970, ApJ, 160, 811.
- Frenk C.S., White S.D.M., Davis M., Efstathiou G., 1988, ApJ, 327, 507.
- Field G.B., Goldsmith D.W., Habing H.J., 1969, ApJ, 155, L149.
- Gnedin N.Y., Ostriker J.P., 1997, ApJ, 486, 581.
- Goldreich P., Lynden-Bell D., 1965, MNRAS, 130, 125.
- Gunn J.E., 1982, in *Astrophysical Cosmology*, eds H.A. Bruck, G.V. Coyne and M.S. Longair, Pontificia Academia Scientiarum, p233.
- Haiman Z., Rees M.J., Loeb A., 1997, ApJ, 483, 21.
- Haiman Z., Abel T., Rees M.J., 1999, ApJ, submitted. astro-ph/9903336.
- Heckman T.M., Armus L., Miley G.K., 1990, ApJS, 74.
- Hernquist L., Katz N., Weinberg D.H., Miralda-Escude J., 1996, ApJ, 457, L51.
- Holmberg E., 1958, Medd-Lunds astr. Obs. Ser, II, 136.
- Holzer T.E., Axford W.I., 1970, ARAA, 8, 31.
- Jog C.J., Solomon P.M., 1984, ApJ, 276, 114.
- Kahn F.D., 1991, *Investigating the Universe*, ed. F.D. Kahn, Reidel, Dordrecht, p1.
- Katz N., 1992, ApJ, 391, 502.
- Kauffmann G., 1996, MNRAS, 281, 475.
- Kauffmann G., White S.D.M., Guiderdoni B., 1993, MNRAS, 263, 201.
- Kauffmann G., Charlot S., 1994, ApJ, 430, L97.
- Kauffmann G., Guiderdoni B., White S.D.M., 1994, MNRAS, 267, 981.
- Kennicutt R.C., 1998, in *The Interstellar Medium in Galaxies*, ed. J.M. Van der Hulst, Kluwer Academic Publishers, Dordrecht. p171.
- Lacey C., Fall S.M., 1983, MNRAS, 204, 791.
- Lacey C., Fall S.M., 1985, ApJ, 290, 154.
- Lacey C., Guiderdoni B., Rocca-Volmerange B., Silk J., 1993, ApJ, 402, 15.
- Larson R.B., 1974, MNRAS, 169, 229.
- Loveday J., Peterson B.A., Efstathiou G., Maddox S.J., 1992, ApJ, 390, 338.
- Mac Low M., Ferrara A., 1999, ApJ, 513, 142.
- Madau P., Della Valle M., Panagia N., 1998, MNRAS, 297, L17.
- Maddox S.J., *et al.* 1998, in *Large-Scale Structure: Tracks and Traces*. Proceedings of the 12th Potsdam Cosmology Workshop. Eds V. Mueller, S. Gottloeber, J.P. Muecket, J. Wambsganss. World Scientific p91.
- McKee C.F., Ostriker J.P., 1977, ApJ, 218, 148. (MO77).
- Mihalas D., Binney J.J., 1981, *Galactic Astronomy* 2nd Edition, Freeman, San Francisco.
- Mo H.J., Miralda-Escude J., 1994, ApJ, 430, L25.
- Moore B., Ghigna S., Governato F., Lake G., Quinn T., Stadel J., Tozzi, 1999, ApJL, in press. astro-ph/9907411.
- Murray S.D., White S.D.M., Blondin, J.M., Lin D.N.C., ApJ, 1993, 407, 588.
- Mushotsky R., Loewenstein M., 1997, ApJ, 481, L63.
- Navarro J.F., Benz W., 1991, ApJ, 380, 320.
- Navarro J.F., White S.D.M., 1993, MNRAS, 265, 271.
- Navarro J.F., Frenk C.S., White S.D.M., 1996, ApJ, 462, 536.
- Navarro J.F., Steinmetz M., 1997, ApJ, 478, 13.
- Navarro J.F., Steinmetz M., 2000, ApJ, submitted. astro-ph/0001003.
- Nulsen P.E.J., Barcons X., Fabian A.C., 1998, MNRAS, 301, 168.
- Pagel B.E., 1997, *Nucleosynthesis and Chemical Evolution of Galaxies*, Cambridge University Press, Cambridge.
- Pei Y.C., Fall M., Hauser M.G., 1999, ApJ, 522, 604.
- Pettini M., 1999, astro-ph/9902173.
- Pettini M., Smith L.J., King D.L., Hunstead R.W., 1997, ApJ, 486, 665.
- Pettini M., Steidel C.C., Adelberger K.L., Dickinson M., Giavalisco M., 2000, ApJ, in press. astro-ph/9910144.
- Pettini M., Ellison S.L., Steidel, C.C., Bowen D.V., 1999, ApJ, 510, 576.
- Pitts E., Tayler R.J., 1989, MNRAS, 240, 373.
- Press W.H., Schechter P., 1974, ApJ, 193, 437.
- Quinn T., Katz N., Efstathiou G., 1996, MNRAS, 278, L49.
- Rees M.J., Ostriker J.P., 1977, MNRAS, 179, 541.
- Salpeter E.E., 1955, ApJ, 121, 161.
- Shapiro P.R., Field G.B., 1976, ApJ, 205, 762.
- Silk J., 1997, ApJ, 481, 703.
- Silk J. and Rees M.J., 1998, AA, 331, L1.
- Somerville R.S., Primack J.R., 1999, MNRAS, 310, 1087.
- Spitzer L., 1968, in *Stars and Stellar Systems Vol VII*, eds. B. Middlehurst and L.H. Adler, University of Chicago Press, p1.
- Storrie-Lombardi L., McMahon R., Irwin M., 1996, MNRAS, 283, L79.
- Strickland D.K., Stevens I.R., 1999, MNRAS, in press.
- Talbot R.J., Arnett W.D., 1975, ApJ, 197, 551.
- Theuns T., Leonard A., Efstathiou G., Pearce F.R., Thomas P.A., 1998, MNRAS, 301, 478.
- Toomre A., 1964, ApJ, 139, 1217.
- Vader P.J., 1986, ApJ, 305, 669.
- Vader P.J., 1987, ApJ, 317, 128.
- Vila-Costas M.B., 1998, in *The Interstellar Medium in Galaxies*, ed. J.M. Van der Hulst, Kluwer Academic Publishers, Dordrecht. p153.
- Vila-Costas M.B. and Edmunds M.G., 1992, MNRAS, 259, 121.
- Wang B., 1995a, ApJ, 444, 590.
- Wang B., 1995b, ApJ, 444, L17.
- Warren M.S., Quinn P.J., Salmon J.K., Zurek W.H., 1992, ApJ, 399, 405.
- Watson G.N., 1944, *A Treatise on the Theory of Bessel Functions*, 2nd Edition, Cambridge University Press, Cambridge.
- Weil M., Eke V.R., Efstathiou G., 1998, MNRAS, 300, 773.
- White S.D.M., Rees M.J., 1978, MNRAS, 183, 341.
- White S.D.M., Frenk C.S., 1991, ApJ, 379, 52.

Wolfe A.M., 1995, in *QSO Absorption Lines*, Ed. G. Meylan, Springer-Verlag, Heidelberg, p13.
 Wolfire M.G., Hollenbach D., McKee C.F., Tielens A.G.G.M., Bakes E.L.O., 1995, ApJ, 443, 152.
 Zucca E., *et al.* 1997, A&A, 326, 477.

APPENDIX A: FAST COMPUTATION OF THE ROTATION CURVE OF A THIN DISC

We begin with the expression for the potential of a thin disc at $z = 0$

$$\phi(r, z = 0) = -2\pi G \int_0^\infty \int_0^\infty J_0(kr) J_0(kr') r' \mu(r') dr' dk. \quad (\text{A1})$$

The integral over k is a well-known discontinuous integral (*e.g.* Watson 1944)

$$\int_0^\infty J_0(kr) J_0(kr') dk = \frac{2}{\pi} \begin{cases} (1/r)K(r'/r) & r' < r \\ (1/r')K(r/r') & r' > r \end{cases} \quad (\text{A2})$$

where K is the complete elliptic integral of the first kind. Differentiating equation (A2), we find

$$v^2(r) = 4Gr \left\{ \int_0^{r-\epsilon} I_<(r, r') r' \mu(r') dr' + \int_{r+\epsilon}^\infty I_>(r, r') r' \mu(r') dr' \right\}, \quad (\text{A3a})$$

$$I_<(r, r') = \frac{E(r'/r)}{(r^2 - r'^2)}, \quad (\text{A3b})$$

$$I_>(r, r') = \frac{K(r/r')}{rr'} - \frac{r'E(r/r')}{r(r'^2 - r^2)}, \quad (\text{A3c})$$

where E is the complete elliptic integral of the second kind. This integral is convergent in the limit $\epsilon \rightarrow 0$. The functions $I_<$ and $I_>$ can be evaluated once and stored, reducing the computation of $v^2(r)$ to a simple integral over the surface density of the disc multiplied by the tabulated functions. We evaluate the epicyclic frequency by differentiating equation (A3) numerically.

APPENDIX B: STEADY SPHERICAL WINDS

The equations governing a steady spherically symmetric wind are

$$\frac{1}{r^2} \frac{d}{dr} (\rho v r^2) = q(r), \quad (\text{B1a})$$

$$\rho v \frac{dv}{dr} = -\frac{dp}{dr} - \rho \frac{d\Phi}{dr} - q(r)v, \quad (\text{B1b})$$

$$\frac{1}{r^2} \frac{d}{dr} \left[\rho v r^2 \left(\frac{1}{2} v^2 + \frac{5}{2} \frac{p}{\rho} \right) \right] + \rho v \frac{d\Phi}{dr} = \mathcal{H} - \mathcal{C}, \quad (\text{B1c})$$

where $q(r)$ is the mass density injected per unit time and \mathcal{H} and \mathcal{C} are the heating and cooling rates per unit volume (*e.g.* Burke 1968, Holzer and Axford 1970). We assume that the gravitational force is given by the NFW halo potential (equation 3), $d\Phi/dr = v_H^2(r)/r$, and rewrite these equations as two dimensionless first order equations

$$\frac{dv^2}{dx} = \frac{1}{2\pi x^2 (c^2 - v^2)} \left[-8\pi x c^2 v^2 + 4\pi x v^2 v_H^2 \right.$$

$$\left. + \frac{4}{3} \gamma v^2 + \gamma c_i^2 - \frac{2}{3} \kappa \right] \quad (\text{B2a})$$

$$\frac{dc^2}{dx} = \frac{-1}{6\pi x^2 (c^2 - v^2) v^2} \left[-8\pi x c^2 v^4 + 4\pi x c^2 v^2 v_H^2 \right.$$

$$\left. -\gamma (v^2 c^2 - \frac{3}{2} c^4 - \frac{5}{6} v^4) - \frac{3}{2} \gamma c_i^2 (c^2 - \frac{5}{3} v^2) + \kappa (c^2 - \frac{5}{3} v^2) \right] \quad (\text{B2b})$$

where c is the adiabatic sound speed, $x = r/r_v$, and all velocities are expressed in units of v_v . The quantities γ and κ in these equations are related to the mass injection and cooling rates according to

$$\gamma(x, v) = \frac{q(r) \dot{M}(r)}{\rho^2 r_v v_v^2}, \quad \kappa(x, c) = \frac{\dot{M}(r) \Lambda(T) n_e^2}{\rho^2 v_v^4 r_v},$$

$$\dot{M}(r) = 4\pi \int_0^r q(r') r'^2 dr. \quad (\text{B2c})$$

and the injected gas is assumed to have a uniform initial isothermal sound speed of $c_i = (kT_i / (0.61 m_p))^{1/2}$.

We illustrate the behaviour of the wind solutions by studying two regimes. Firstly, we assume that $q = 0$ beyond an initial radius $r_i = 0.04 r_v$ defining the base of the flow (*i.e.* two disc scale lengths for $f_{coll} = 50$). Equations (B2) do not have a transonic point when $q = 0$ (Wang 1995a, see also the discussion below) and so we begin the integrations at a Mach number slightly greater than unity with $c^2 = 5c_i^2/3$. We adopt the parameters of models MW and DW given in Table 1 and integrate the equations (B1) adopting $\dot{M} = 10 M_\odot/\text{yr}$ for model MW and $\dot{M} = 0.2 M_\odot/\text{yr}$ for model DW. These mass injection rates are close to the maximum rates at times $t \sim \tau_{ej}$ for the models described in Section 6. The curves in Figure B1 show solutions for initial isothermal sound speeds of 0.75, 1.0 and 1.25 times the escape velocity from the centre of the halo ($v_{esc} = 430 \text{ kms}^{-1}$ for model MW and 107 kms^{-1} for model DW).

The figure shows that the criterion $v_w \approx \sqrt{2.5} c_i \gtrsim v_{esc}$ is about right if the wind is to reach beyond the virial radius. For $c_i \approx v_{esc}$ the wind in model MW begins at a high temperature of $T_i \approx 1.4 \times 10^7 \text{ K}$ and cools almost adiabatically initially, reaching a temperature of $\sim 1.5 \times 10^5 \text{ K}$ at the virial radius. The timescale for the flow to reach the virial radius, $\sim 2 \times 10^8 \text{ yrs}$, is slightly longer than the cooling time at r_v . The behaviour of models DW is quite different. For $c_i \approx v_{esc}$ the initial temperature of the gas is $T_i \approx 8 \times 10^5 \text{ K}$ and cools to $\lesssim 10^4 \text{ K}$ by $r = 0.3 r_v$. As expected from the discussion in Section 6, cooling is important in outflows from dwarf galaxies (see *e.g.* Kahn 1981, Wang 1995a, b).

An investigation of transonic solutions of equations (B2) require a model for $q(r)$. An example is illustrated in Figure B2 for model DW, using

$$q(r) = \frac{\dot{M}(\infty)}{8\pi r_w^3} \exp(-r/r_w), \quad r_w = 0.04 r_v. \quad (\text{B3})$$

In this solution, $\dot{M}(\infty) = 0.2 M_\odot/\text{yr}$ and the central gas density was adjusted to obtain a critical solution for the case $c_i = v_{esc}$. If the gas is to escape from a dwarf galaxy the transonic point must occur before cooling sets in. For such systems, the wind parameters would adjust so that a sonic point exists at a characteristic cooling scale height as shown in Figure B2. The wind will then cool radiatively just beyond the sonic point forming a cold wind as discussed above. It is also likely that the wind will be heated to a temperature of

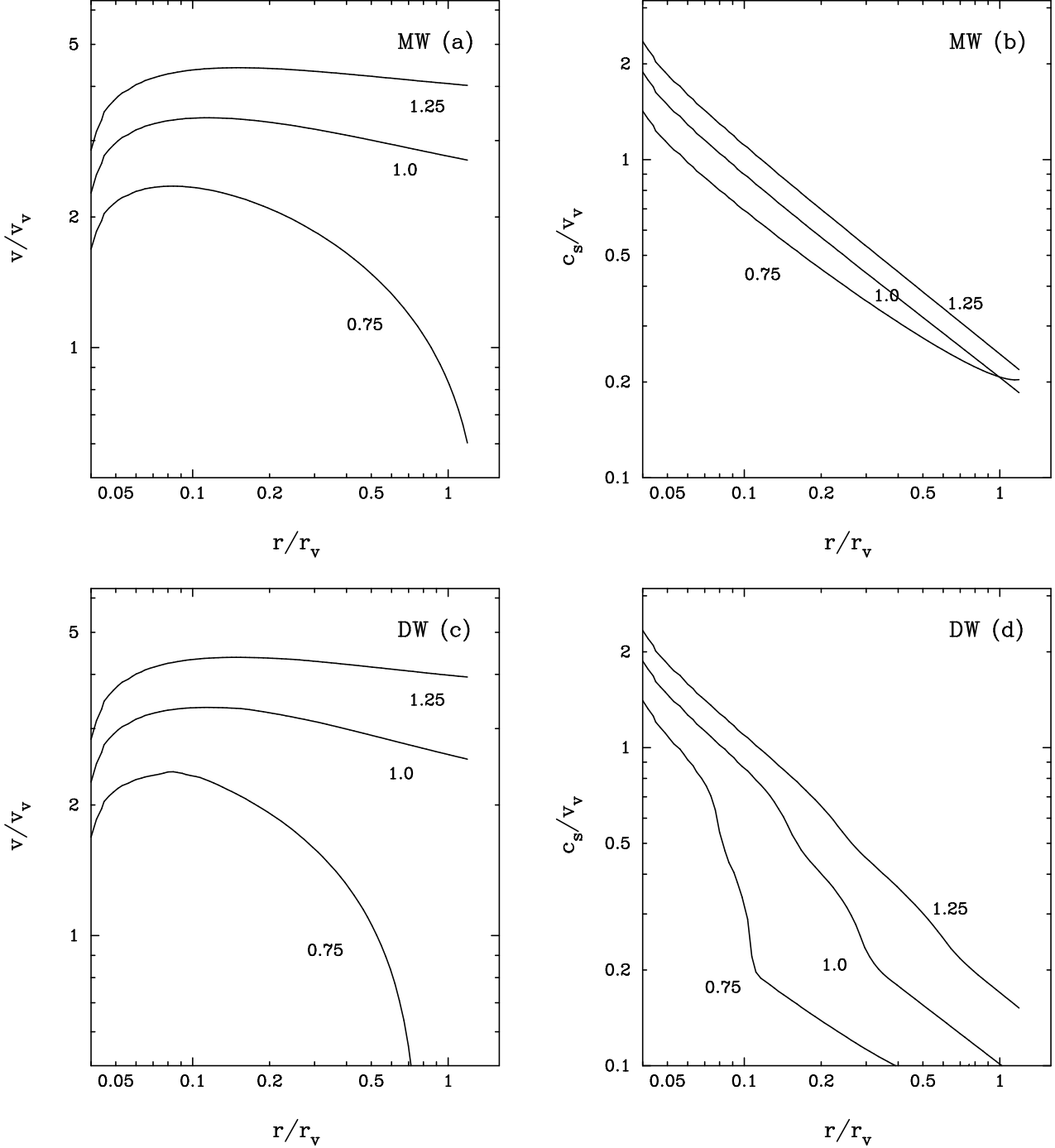


Figure B1. Steady wind solutions for models MW and DW including radiative cooling. The curves show the wind velocity (figs a,c) and adiabatic sound speed (figs b, d) assuming that the flow begins at $r_i = 0.04r_v$ with a Mach number of unity. The numbers give the initial isothermal sound speed in units of the escape speed v_{esc} from the centre of the halo. These curves are for a mass injection rate of $10M_{\odot}/\text{yr}$ for model MW and $0.2M_{\odot}/\text{yr}$ for model DW.

$T \sim 10^4\text{K}$ by photoionizing radiation from the galaxy and the general UV background. These sources of heating have not been included in the models of Figures B1 and B2.

The wind will be thermally unstable when cooling sets in, and may form clouds. However, in the absence of a confining medium, the clouds would have a filling factor of order unity so the wind is likely to maintain its integrity until it

meets the surrounding IGM. The external pressure required to balance the ram pressure of the wind is

$$\frac{p_{ext}}{k} \approx 80 \left(\frac{\dot{M}}{0.2M_{\odot}/\text{yr}} \right) \left(\frac{r}{10 \text{ kpc}} \right)^{-2} \times \left(\frac{v_w}{100 \text{ km/s}} \right) \text{ cm}^{-3} \text{ K}, \quad (\text{B4})$$

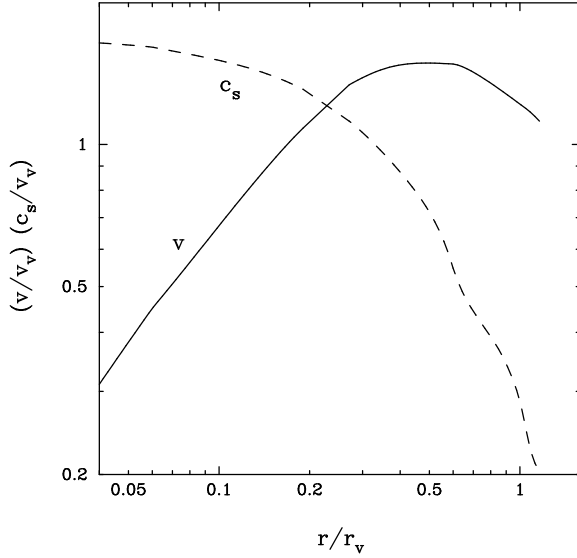


Figure B2. Critical solution for a wind in model DW with $c_i = v_{esc}$, $\dot{M}(\infty) = 0.2M_{\odot}/\text{yr}$, and $q(r)$ given by equation (B3).

which is about equal to the pressure of the IGM with a temperature of 10^4K and an overdensity of

$$\Delta \approx 4500 \left(\frac{2}{1+z} \right)^3 T_4^{-1} \left(\frac{\dot{M}}{0.2M_{\odot}/\text{yr}} \right) \times \left(\frac{r}{10 \text{ kpc}} \right)^{-2} \left(\frac{v_w}{100 \text{ km/s}} \right). \quad (\text{B5})$$

Provided that the halo is devoid of high pressure gas, the cool wind will propagate beyond the virial radius and will be halted either by the ram pressure of infalling gas or after sweeping up a few times its own mass. As pointed out by Babul and Rees (1992), if a dwarf galaxy is embedded in a group or cluster of galaxies with a pressure exceeding $\sim 100 \text{ cm}^{-3}\text{K}$, the bulk motion of the outflowing gas would be thermalized in a shock and the cooled shocked gas could fall back onto the galaxy generating a new burst of star formation. The efficiency of feedback is therefore likely to be a function of local environment.